THE JOURNAL OF BIOLOGICAL CHEMISTRY VOL. 290, NO. 42, pp. 25670–25685, October 16, 2015
Published in the U.S.A.

Loss of a Functionally and Structurally Distinct LD-Transpeptidase, Ldt_{Mt5}, Compromises Cell Wall Integrity in *Mycobacterium tuberculosis*[*]

Received for publication, May 29, 2015, and in revised form, August 20, 2015 Published, JBC Papers in Press, August 24, 2015, DOI 10.1074/jbc.M115.660753

Leighanne A. Brammer Basta[‡§1], Anita Ghosh[¶], Ying Pan[¶], Jean Jakoncic[‖], Evan P. Lloyd[**], Craig A. Townsend[**], Gyanu Lamichhane[‡§2], and Mario A. Bianchet[¶‡‡3]

*From the [‡]Taskforce to study Resistance Emergence and Antimicrobial development Technology (TREAT) and [§]Division of Infectious Diseases, The Johns Hopkins University School of Medicine, Baltimore, Maryland 21231, [¶]Structural Enzymology and Thermodynamics Group, Department of Biophysics and Biophysical Chemistry and [‡‡]Department of Neurology, The Johns Hopkins University School of Medicine, Baltimore, Maryland 21205, [‖]National Synchrotron Light Source II, Brookhaven National Laboratory, Upton, New York 11973, and **Department of Chemistry, The Johns Hopkins University, Baltimore, Maryland 21218*

Background: *M. tuberculosis* Ldt_{Mt5} is an Ldt_{Mt2} paralog that cross-links peptidoglycan stem peptides.
Results: Ldt_{Mt5} is structurally divergent, strains lacking Ldt_{Mt5} are more susceptible to chemical and environmental stresses, and Ldt_{Mt2} cannot compensate for its loss.
Conclusion: Ldt_{Mt2} and Ldt_{Mt5} serve non-redundant roles in peptidoglycan maintenance.
Significance: Ldt_{Mt5} is necessary for properly maintaining cell wall integrity and should be pursued as a drug target.

The final step of peptidoglycan (PG) biosynthesis in bacteria involves cross-linking of peptide side chains. This step in *Mycobacterium tuberculosis* is catalyzed by LD- and DD-transpeptidases that generate 3⟶3 and 4⟶3 transpeptide linkages, respectively. *M. tuberculosis* PG is predominantly 3⟶3 cross-linked, and Ldt_{Mt2} is the dominant LD-transpeptidase. There are four additional sequence paralogs of Ldt_{Mt2} encoded by the genome of this pathogen, and the reason for this apparent redundancy is unknown. Here, we studied one of the paralogs, Ldt_{Mt5}, and found it to be structurally and functionally distinct. The structures of apo-Ldt_{Mt5} and its meropenem adduct presented here demonstrate that, despite overall architectural similarity to Ldt_{Mt2}, the Ldt_{Mt5} active site has marked differences. The presence of a structurally divergent catalytic site and a proline-rich C-terminal subdomain suggest that this protein may have a distinct role in PG metabolism, perhaps involving other cell wall-anchored proteins. Furthermore, *M. tuberculosis* lacking a functional copy of Ldt_{Mt5} displayed aberrant growth and was more susceptible to killing by crystal violet, osmotic shock, and select carbapenem antibiotics. Therefore, we conclude that Ldt_{Mt5} is not a functionally redundant LD-transpeptidase, but rather it serves a unique and important role in maintaining the integrity of the *M. tuberculosis* cell wall.

Virtually all bacteria possess a peptidoglycan (PG)[4] layer that encapsulates the cytoplasmic membrane and provides shape and rigidity to the cell. Considered as a vital bacterial "organelle," the PG is essential for cellular growth and viability. β-Lactams, the class of drugs with the highest impact in treating bacterial infections in humans (1), act by inhibiting PG biosynthesis (2).

Mature PG comprises aminosugar strands with alternating *N*-acetylmuramic acid and *N*-acetylglucosamine units and peptide moieties that are cross-linked to one another (3). Lipid II, a precursor to PG, is synthesized intracellularly and consists of a single disaccharide-peptide and lipid moiety. In *Mycobacterium tuberculosis*, the infectious pathogen that causes tuberculosis, the pathway for lipid II biosynthesis comprises more than 20 genes, and all are essential for the viability of this pathogen (4). Lipid II is transported across the membrane, and units are linked together by transglycosylases that extend the aminosugar strand. The final step in PG maturation involves cross-linking the peptide moieties to one another by both DD- and LD-transpeptidases.

Until recently, the PG was considered to be largely cross-linked by DD-transpeptidases that generate 4⟶3 transpeptide linkages between the fourth amino acid (D-alanine) of one chain and the third amino acid (*meso*-diaminopimelic acid in *M. tuberculosis*) of an adjacent chain. Interestingly, the majority of transpeptide linkages in *Mycobacterium* spp. are between *meso*-diaminopimelic acid residues of two peptide chains (5). These 3⟶3 linkages are formed by LD-transpeptidases (6, 7), and the dominant LD-transpeptidase in *M. tuberculosis* is Ldt_{Mt2} (8). Unlike DD-transpeptidases that utilize a catalytic ser-

* This work was supported, in whole or in part, by National Institutes of Health Grant DP2OD008459 (to G. L.). The authors declare that they have no conflicts of interest with the contents of this article.
The atomic coordinates and structure factors (codes 4Z7A and 4ZFQ) have been deposited in the Protein Data Bank (http://wwpdb.org/).
[1] Present address: Chemistry Dept., United States Naval Academy, Annapolis, MD 21402.
[2] To whom correspondence may be addressed: The Johns Hopkins University School of Medicine, 1503 E. Jefferson St., Baltimore, MD 21231. Tel.: 410-502-8162; E-mail: lamichhane@jhu.edu.
[3] To whom correspondence may be addressed: Depts. of Neurology and Biophysics and Biophysical Chemistry, The Johns Hopkins University School of Medicine, 725 N. Wolfe St., Baltimore, MD 21205. Tel.: 410-614-8221; E-mail: bianchet@jhmi.edu.

[4] The abbreviations used are: PG, peptidoglycan; ITC, isothermal titration calorimetry; TCEP, tris(2-carboxyethyl)phosphine; Blg, bacterial Ig-like; CTSD, C-terminal subdomain; CD, catalytic domain; ex-CTSD, extension of the C-terminal subdomain; TEV, tobacco etch virus; r.m.s., root mean square; r.m.s.d., root mean square deviation; Tn, transposon; EYY, ErfK/YbiS/YhnG.

TABLE 1
Summary of primers used
Restriction sites are underlined. F, forward primer; R, reverse primer.

Gene/variant	Primers
ldt_{Mt5}	F, 5′-TATTGCCATATGAAGCTGGCCGAGAAGAGG-3′ R, 5′-TATTGCCTCGAGCTACCCACCCGGTCCGTT-3′
H342A Ldt_{Mt5}	F, 5′-CAACAACGGCGAGTTCATCGCTG CCAACCCTATGAGCGCC-3′ R, 5′-GGCGCTCATAGGGTTGGCAGCGATGAACTCGCCGTTGTTG-3′
H342Q Ldt_{Mt5}	F, 5′-CAACAACGGCGAGTTCATCCAGGCCAACCCTATGAGCGCC-3′ R, 5′-GGCGCTCATAGGGTTGGCCTGGATGAAC TCGCCGTTGTTG-3′
M346W Ldt_{Mt5}	F, 5′-GAGTTCATCCATGCCAACCCTTGGAGCGCCGGTGCCCAGGGCAAC-3′ R, 5′-GTTGCCCTGGGCACCGGCGCTCCAAGGGTTGGCATGGATGAACTC-3′
T357V Ldt_{Mt5}	F, 5′-CAGGGCAACAGCAATGTCGTCAACGGCTGTATCAACCTGTCG-3′ R, 5′-CGACAGGTTGATACAGCCGTTGACGACATTGCTGTTGCCCTG-3′
N358A Ldt_{Mt5}	F, 5′-GGCAACAGCAATGTCACCGCCGGCTGTATCAACCTGTCGACG-3′ R, 5′-CGTCGACAGGTTGATACAGCCGGCGGTGACATTGCTGTTGCC-3′
N358H Ldt_{Mt5}	F, 5′-CAGGGCAACAGCAATGTCACCCACGGCTGTATCAACCTGTCGACG-3′ R, 5′-CGTCGACAGGTTGATACAGCCGTGGGTGACATTGCTGTTGCCCTG-3′
C360A Ldt_{Mt5}	F, 5′-CAGCAATGTCACCAACGGCGCTATCAACCTGTCGACGGAG-3′ R, 5′-CTCCGTCGACAGGTTGATAGCGCCGTTGGTGACATTGCTG-3′
N362A Ldt_{Mt5}	F, 5′-GTCACCAACGGCTGTATCGCCCTGTCGACGGAGAACGCC-3′ R, 5′-GGCGTTCTCCGTCGACAGGGCGATACAGCCGTTGGTGAC-3′

ine and pentapeptide substrates (9), LD-transpeptidases require a catalytic cysteine residue (10, 11) and utilize tetrapeptide substrates. LD-Transpeptidation has now been identified in a range of pathogenic bacteria (11–13), highlighting the importance of this fundamental mechanism across bacterial species.

In *M. tuberculosis*, loss of Ldt_{Mt2} results in altered cell size, growth, and virulence as well as loss of the ability of the organism to secrete low molecular weight proteins and increased susceptibility to amoxicillin (8, 14). The genome of *M. tuberculosis* encodes four additional paralogs of Ldt_{Mt2}. On the basis of *in vitro* cross-linking activity or sequence similarity, they have been annotated as Ldt_{Mt1} (Rv0116c), Ldt_{Mt3} (Rv1433), Ldt_{Mt4} (Rv0192), and Ldt_{Mt5} (Rv0483) and share amino acid sequence identity of 36, 34, 35, and 28% with Ldt_{Mt2}, respectively. It is unclear whether the five sequence paralogs are functionally redundant.

We used a combination of biophysical, biochemical, and genetic approaches to study Ldt_{Mt5}. Here, we report the first crystal structures of apo- and meropenem-bound Ldt_{Mt5} and describe the phenotypic effects on *M. tuberculosis* lacking this enzyme. Our data indicate that Ldt_{Mt5} is structurally divergent compared with other *M. tuberculosis* LD-transpeptidases and that this protein serves a critical and distinct role in proper maintenance of *M. tuberculosis* cell wall integrity, highlighting its potential as a novel drug target.

Experimental Procedures

General Methods—All reagents were obtained from commercial sources. Spectrophotometric analyses were performed on a Shimadzu UV-1800 UV-visible spectrophotometer. Primers were purchased from Integrated DNA Technologies. Isothermal titration calorimetry (ITC) experiments were performed using a high precision VP-ITC titration calorimeter system (Microcal Inc.). Ultraperformance liquid chromatography (LC)-high resolution MS samples were analyzed on a Waters Acquity H-Class ultraperformance LC system equipped with a multiwavelength ultraviolet-visible diode array detector in conjunction with a Waters Acquity BEH-300 ultraperformance LC column packed with a C_4 stationary phase (2.1 × 50 mm; 1.7 μm) in tandem with high resolution MS analysis by a Waters Xevo-G2 quadrupole-TOF electrospray ionization mass spectrometer. Molecular graphics and analyses were performed with the UCSF Chimera package. Chimera is developed by the Resource for Biocomputing, Visualization, and Informatics at the University of California, San Francisco (supported by National Institutes of Health NIGMS Grant P41-GM103311).

Cloning, Overexpression, and Purification of Ldt_{Mt5}—A truncated version of ldt_{Mt5} (encoding amino acids 55–451) was amplified by PCR (1× New England Biolabs GC reaction buffer, 200 μM dNTPs, 2 ng/μl CDC1551 *M. tuberculosis* genomic DNA, 500 nM primers (Table 1), 1 unit of Phusion polymerase, and 3% DMSO), digested with NdeI and XhoI, and cloned into a modified pET28a vector that encodes for a TEV-cleavable N-terminal His_6 tag (10). *Escherichia coli* BL21(DE3) cells harboring the ldt_{Mt5}-pET28a plasmid were grown to an A_{600} of ~0.5 at 37 °C. Flasks were then cooled on ice with periodic shaking. Protein overexpression was induced with 100 μM isopropyl 1-thio-β-D-galactopyranoside, and flasks were returned to an incubator shaker at 16 °C for an additional 24 h. Cells were harvested at 4 °C and stored overnight at −20 °C. Thawed cells were resuspended in protein purification buffer (25 mM Tris, pH 8.0, 400 mM NaCl, 10% glycerol, and 1 mM tris(2-carboxyethyl)phosphine (TCEP)) and protease inhibitor mixture (Roche Applied Science) and lysed by ultrasonication, and cell debris was removed by centrifugation at 4 °C. The supernatant was incubated with nickel-nitrilotriacetic acid resin at 4 °C for 90 min, and His_6-tagged Ldt_{Mt5} was eluted from the resin over a stepwise gradient of 5–500 mM imidazole. Fractions containing Ldt_{Mt5} (as determined by SDS-PAGE) were combined, and protein concentration was determined using the Bio-Rad Protein Assay with bovine serum albumin (BSA) as a standard. The sample was then subjected to dialysis overnight at 4 °C against 1 liter of 25 mM Tris, pH 8.0, 100 mM NaCl, 10% glycerol, and 1 mM TCEP in the presence of TEV protease (1:100 TEV:Ldt_{Mt5}).

Following dialysis, the TEV-treated sample was incubated with fresh nickel-nitrilotriacetic acid resin at 4 °C for 90 min. Cleaved Ldt_{Mt5} was collected as flow-through, whereas the His-tagged TEV protease and cleaved His_6 tag remained bound to the resin. Ldt_{Mt5} was subjected to a second dialysis against 1 liter of 25 mM Tris, pH 8.0, 100 mM NaCl, and 1 mM TCEP for 4 h at 4 °C. The concentration of Ldt_{Mt5} was determined using the Bio-Rad Protein Assay with BSA as a standard, and Ldt_{Mt5} was concentrated to 12.8 mg/ml prior to being flash frozen in liquid N_2. Protein was stored at −80 °C.

Site-directed Mutagenesis Studies—Site-directed mutagenesis reactions were performed as described previously with minor modifications (15). Briefly, two PCRs (25 μl) containing either the forward or reverse primer were set up in parallel. Each PCR contained 1× New England Biolabs GC reaction buffer, 200 μM dNTPs, 1 ng/μl template, a 500 nM concentration of either the forward or reverse primer, 1 unit of Phusion polymerase, and 3% DMSO. The *ldt_{Mt5}*-pET28a plasmid was used as the template to generate each Ldt_{Mt5} variant (see Table 1 for primers). Sufficient elongation of primer at 68 °C occurred over 15 min. Forward and reverse PCRs were then combined (new volume of 50 μl), and complementary strands were reannealed following gradual cooling (95 °C, 5 min; 90 °C, 1 min; 80 °C, 1 min; 70 °C, 30 s; 60 °C, 30 s; 50 °C, 30 s; and 40 °C, 30 s). Samples were then incubated at 37 °C, and template DNA was digested with 1 unit of DpnI for 3 h. All constructs were fully sequenced, and competent bacteria were transformed with mutagenic plasmid. All variants were purified as described above.

Kinetic Analyses—The nitrocefin hydrolytic activities of Ldt_{Mt2}, Ldt_{Mt5}, and Ldt_{Mt5} variants were measured spectrophotometrically as reported previously for Ldt_{Mt2} (10) but with modifications. Briefly, reaction mixtures containing 1× tribuffer (100 mM MES, 50 mM *N*-ethylmorpholine, and 50 mM diethanolamine, pH 10), 0.1 mg/ml BSA, 100 mM NaCl, 1 mM TCEP, 5% DMSO, and 10 μM Ldt_{Mt5} or Ldt_{Mt5} variant were preincubated at 37 °C for 5 min. Nitrocefin (Calbiochem) was added to initiate each reaction, and the rate of nitrocefin hydrolysis was measured at 486 nm at 37 °C. For each set of reactions, the rate of nitrocefin hydrolysis in the absence of enzyme was observed and was subtracted from the initial rate of nitrocefin hydrolysis in the presence of enzyme at each substrate concentration. Initial rates of nitrocefin hydrolysis were measured over 3 min. An extinction coefficient (ϵ_M) of 20,500 $M^{-1}\,cm^{-1}$ was used in determining the concentration of hydrolyzed nitrocefin as it was experimentally determined that ϵ_M does not change with changing pH under these buffering conditions (data not shown). Non-linear regression analyses of initial velocities were performed using GraphPad Prism (version 5). Reaction mixtures containing nitrocefin (100 μM) and Ldt_{Mt5} or Ldt_{Mt2} (5 μM) at varying pH values in 1× tribuffer and the conditions described above were monitored spectrophotometrically for determining the optimal pH for each enzyme. To rule out the possibility that residual TEV incompletely removed during protein purification could be contributing to nitrocefin hydrolysis at pH 10, we evaluated nitrocefin as a substrate for TEV at pH 10. Only baseline levels of hydrolysis were observed, indicating that TEV was not significantly contributing to the observed rates of hydrolysis by Ldt_{Mt5} and Ldt_{Mt5} variants (data not shown). Conversely, when we evaluated nitrocefin as a substrate for His_6-Ldt_{Mt5}, we observed rates of hydrolysis that were comparable with TEV-cleaved Ldt_{Mt5} (data not shown).

Mass Spectrometry Analyses—Ldt_{Mt5} or N358H/M346W Ldt_{Mt5} (2 μM) in 12.5 mM Tris buffer, pH 8 was incubated in the presence or absence of 50 μM carbapenem for 5 h at room temperature. Reactions were quenched by the addition of trifluoroacetic acid (TFA; final concentration, 0.1%). Samples were filtered through a 0.2-μm filter and analyzed by ultraperformance LC/MS at 60 °C. The mobile phase was as follows: 0–1 min, isocratic 90% water + 10% ACN + 0.1% formic acid; 1–7.5 min, gradient to 20% water + 80% ACN + 0.1% formic acid; 7.5–8.4 min, isocratic 20% water + 80% ACN + 0.1% formic acid; 8.4–8.5 min, gradient to 90% water + 10% ACN + 0.1% formic acid; 8.5–10 min, isocratic 90% water + 10% ACN + 0.1% formic acid. The flow rate was 0.3 ml min^{-1}.

Crystallization Conditions—Crystals of Ldt_{Mt5} were obtained by the hanging drop vapor diffusion method at 20 °C. Drops of 2 μl of protein (12.8 mg/ml) and 1 μl of reservoir solution were equilibrated against a reservoir containing 85 mM sodium citrate, pH 5.6, 25.5% polyethylene glycol (PEG) 4,000, 170 mM ammonium acetate, and 15% glycerol. Crystals suitable for data collection grew within 1 week. Crystals of Ldt_{Mt5} in complex with meropenem were obtained with protein incubated with the ligand (645 μM) using crystallization conditions identical to that of the apo crystal.

Data Collection, Structure Determination, and Refinement—All diffraction data were collected at beamline X6A of the National Synchrotron Light Source of the Brookhaven National Laboratory (Table 2). X-ray diffraction experiments were carried out with crystals frozen in their respective mother liquor without addition of cryoprotectant. The crystal structure of apo-Ldt_{Mt5} was determined by molecular replacement with the program MOLREP (16) using previously determined Ldt_{Mt2} structures of individual domains as searching models (Protein Data Bank code 3TUR, catalytic domain (CD) and bacterial Ig-like (BIg) B domains; Protein Data Bank code 4HU2, BIgA domain). After 20 cycles of refinement of the three separate domains as rigid bodies with REFMAC (CCP4), the structure was rebuilt with the molecular modeling program Coot (17) and further refined with the program PHENIX using restrained and translation, libration, and screw anisotropic refinement protocols with four translation, libration, and screw groups for each BIg domain and two for the CD (18). The apo-Ldt_{Mt5} structure was refined to a final R_{work} of 0.21 and an R_{free} of 0.255 with 96.1% of the residues in favored stereochemistry regions (Table 2) and solved to 1.98 Å.

The crystal structure of meropenem-bound Ldt_{Mt5} was determined by molecular replacement and refined using a protocol similar to that used when solving the apo-Ldt_{Mt5} structure (Table 2). The partial meropenem adduct was built inside the positive σA ($mF_o - DF_c$) electron density difference map. Weak electron density for the sulfur atom of meropenem was observed, and no electron density for the pyrrolidine ring extension of meropenem was observed. The meropenem adduct structure was refined to an R_{work} of 0.23 and an R_{free} of 0.275 with 93% of the residues in Ramachandran favored

TABLE 2
Statistics of x-ray data collection and structure refinement

	Apo-Ldt_{Mt5}	Meropenem-bound Ldt_{Mt5}
Wavelength (Å)	1.0	1.0
Resolution range (last shell) (Å)	28.92–1.98 (2.051–1.98)	29.04–2.8 (2.9–2.8)
Space group	$P_6 22$	$P_6 22$
Unit cell (Å; °)	101.0, 101.0, 192.7; 90, 90, 120	99.4, 99.4, 193.4; 90, 90, 120
Total reflections	3,529,565	1,838,131
Unique reflections	41,056 (3,985)	14,522 (1,400)
Multiplicity	7.2 (7.0)	22.4 (22.9)
Completeness (%)	99.6 (99.15)	99.4 (98.73)
Mean $I/\sigma(I)$	57.4 (3.9)	53.3 (6.3)
Wilson B-factor	37.81	61.89
R_{sym}	0.048 (0.513)	0.09 (0.9)
Reflections used for R_{free}	2,046	734
R_{work}	0.23 (0.28)	0.23 (0.29)
R_{free}	0.255 (0.36)	0.275 (0.36)
Number of non-hydrogen atoms	2,947	2,750
Protein	2,740	2,669
Ligands	39	32
Water	168	49
Protein residues	355	345
r.m.s.	0.006	0.011
Bonds		
Angles	1.07	1.43
Ramachandran favored (%)	96	93
Ramachandran outliers (%)	0.85	2.6
Clashscore	3.5	9.45
Average B-factor	80	77.0
Protein	80.1	79.8
Ligands	114.3	76
Solvent	70.9	76

regions (Table 2). The structure was solved to 2.8 Å. r.m.s.d. calculations and alignments were performed using the program Molecular Operating Environment (MOE; v.2014.09, GCC Inc.). Additional structural figures were completed using PyMOL (v.1.7.1.3, ©2009–2014 Schrödinger, LLC) and Chimera, v.1.9 (19). Buried surface area calculations were performed using the Protein Interfaces, Surfaces, and Assemblies' Service (PISA) at the European Bioinformatics Institute (20). Coordinates and structure factors were deposited in the Protein Data Bank under the codes 4Z7A (apo-Ldt_{Mt5}) and 4ZFQ (meropenem-bound Ldt_{Mt5}).

Calorimetric Studies—Freshly thawed Ldt_{Mt5} protein was dialyzed overnight in 1 liter of buffer containing 25 mM Tris-HCl, pH 7.5, 100 mM NaCl, and 1 mM TCEP at 4 °C. Dialyzed protein solution was then filtered through a 0.22-μm filter and diluted to 10 μM. The protein concentration was determined by UV absorption at 280 nm using a calculated extinction coefficient of 78,840 M^{-1} cm^{-1}. Freshly thawed aliquots of 20 mM carbapenem stock solutions were diluted to 1 mM in protein dialysis buffer. Protein and ligand solutions were degassed for 20 min in a ThermaVac®. Ligand injections (10 μl) into the cell containing Ldt_{Mt5} were performed with 240-s equilibrations between injections. Data were analyzed with Origin 7 software (OriginLab). All calorimetry experiments were carried out at 27 °C.

M. tuberculosis Strains and Culture Conditions—*M. tuberculosis* CDC1551 (21) (herein referred to as "wild type") was used as the host strain to generate a transposon insertion mutant in the *MT0501* (ldt_{Mt5}::Tn) gene as described previously (22). All strains were grown in Middlebrook 7H9 liquid medium supplemented with 0.2% glycerol, 0.05% Tween 80, 10% (v/v) oleic acid/albumin/dextrose/catalase, 50 μg/ml cycloheximide (herein referred to as 7H9 complete medium), and when indicated 2.0 μg/ml crystal violet. The ldt_{Mt5}::Tn strain was grown in the presence of 20 μg/ml kanamycin. Middlebrook selective 7H11 solid medium (BD Biosciences) was used for enumerating colony forming units (cfus) in *in vitro* growth studies. *M. tuberculosis* H37Rv was used in generating meropenem-resistant strains.

In Vitro Growth and Crystal Violet Studies—All *M. tuberculosis* strains were grown to midexponential phase with an A_{600} of ~0.8 in 7H9 complete medium at 37 °C. Cultures were then diluted to an A_{600} of 0.1 in 7H9 complete medium in the presence or absence of 2.0 μg/ml crystal violet, and turbidity of the cultures was determined daily. Appropriate dilutions of each strain were cultured on Middlebrook 7H11 medium to determine surviving bacilli by enumerating the cfus.

Osmotic Tolerance Studies—Wild-type or ldt_{Mt5}::Tn strains were grown to late exponential phase (A_{600} ~ 2–3) in 7H9 complete medium. Cultures were diluted to an A_{600} of 0.5, and cells were pelleted at low speed. Cells were resuspended in 150 mM NaCl or double distilled H_2O (0 mM NaCl) solutions containing 0.05% Tween 80. Cells were incubated in these conditions for 1 h with shaking at 37 °C. Viability was determined by culturing and enumerating the cfus on 7H11 selective agar.

Determination of Minimum Inhibitory Concentration—Carbapenem minimum inhibitory concentrations were determined using the standard broth dilution method (23). Briefly, 10^5 *M. tuberculosis* bacilli were inoculated into 2.5 ml of 7H9 broth supplemented with 0.2% glycerol, 10% (v/v) oleic acid/albumin/dextrose/catalase, and 50 μg/ml cycloheximide, and the drug was added at different concentrations in the μM–mM range. The cultures were incubated at 37 °C without shaking and evaluated for growth by visual inspection of the broth at 14 and 21 days. Minimum inhibitory concentration values are representative of three independent experiments.

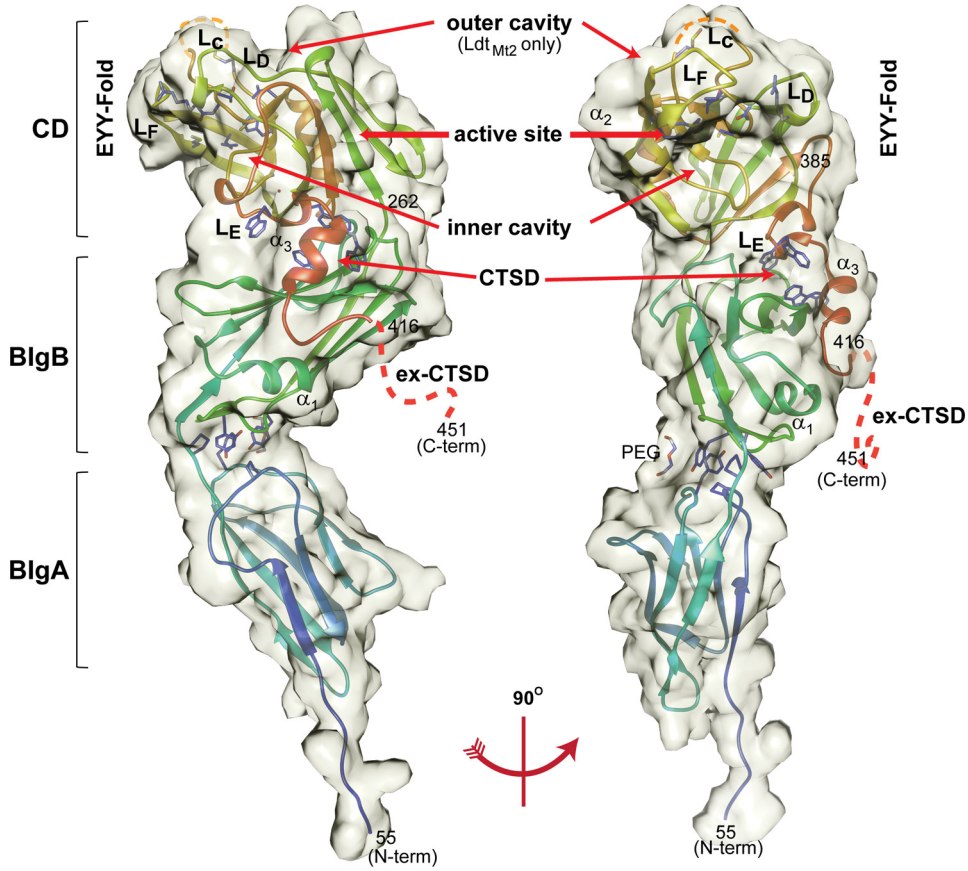

FIGURE 1. **Crystal structure of Ldt_{Mt5}.** *Left*, apo-Ldt_{Mt5}; *right*, rotated 90°. Ldt_{Mt5} is composed of two BIg domains and a CD. The *semitransparent* volume is surface-accessible by a 3.5-Å radius probe. Residues of the active site (His^{342}, Thr^{357}, Asn^{358}, and Cys^{360}) are represented as *sticks* within the CD. Tryptophan residues of the CTSD are also represented as *sticks* and interact with a hydrophobic patch at the interface of the BIgB domain. The prominent outer cavity that is observed in Ldt_{Mt2} is absent in apo-Ldt_{Mt5} but is indicated as a reference (10). The Ldt_{Mt5} secondary structure schematic is colored as a rainbow from *blue* (N terminus) to *red* (C-terminus). *Orange dashes* represent the disordered portion of loop L_C, and *red dashes* represent the disordered ex-CTSD. This figure was made using Chimera (19).

Electron Microscopy Experiments—Field emission scanning electron microscopy and transmission electron microscopy experiments were performed as described previously (14).

Results

Ldt_{Mt5} Structure—The apo and meropenem adduct structures of an N-terminally truncated Ldt_{Mt5} protein lacking the hydrophobic domain predicted to be a membrane anchor for this protein (amino acids 55–451) were determined using x-ray crystallography (Fig. 1). This truncated protein displays higher sequence identity to Ldt_{Mt2} (31%) than the full-length protein does (28%) and includes the proline-rich extension of the C-terminal subdomain (ex-CTSD) comprising residues 417–451 that is absent in all other *M. tuberculosis* LD-transpeptidases (Fig. 2*A*).

Apo-Ldt_{Mt5} and meropenem adduct crystals belong to the $P6_222$ space group with similar cell dimensions and one molecule in the asymmetric unit (Table 2). Electron density for residues 56–346 and 353–416 was observed in the apo crystal form. Residues 347–352 within loop L_C (residues 344–362; nomenclature from Ref. 10) and residues 417 to the C-terminus (residue 451) are disordered; their electron density was not observed in either apo- or meropenem adduct-Ldt_{Mt5} crystal structures. Ldt_{Mt5} possesses three globular domains (Fig. 1) as observed in its paralog Ldt_{Mt2} (Fig. 2*B*) (10, 24–26). The structure reveals an N terminus span of long-chain hydrophilic residues (residues 56–60) that precede two in-tandem antiparallel β-barrels resembling BIg domains joined by a short three-residue linker (BIgA, residues 61–153; BIgB, residues 156–252) followed by a C-terminal CD (residues 253–417). The CD can be divided into a core (residues 253–385) that contains an ErfK/YbiS/YhnG fold (EYY-fold) (27) consisting of a β-sandwich with two mixed β-sheets and one helix (α_2) and a helically folded C-terminal subdomain (CTSD; residues 386–416). LD-Transpeptidases are characterized by the presence of this EYY-folded domain, which contains the characteristic HXX_{14-17}(S/T)HGChN motif (h represents a hydrophobic residue) where cysteine is the catalytic residue (Fig. 2*A*). By extension, we presume Cys^{360} to be the catalytic residue of Ldt_{Mt5}.

The overall structural overlap between apo-Ldt_{Mt5} and Ldt_{Mt2} (Protein Data Bank code 3VYN) has an r.m.s. deviation of 2.2 Å for 225 aligned Cα atoms, including 79 identical residues, highlighting their overall structural similarity (Fig. 2, *B* and *C*). There are small differences with regard to the orientation of the domains among other structurally characterized LD-transpeptidases. The equivalent BIg domains of Ldt_{Mt5} and Ldt_{Mt2} are similar; the BIgA domains display a small r.m.s. deviation of 1.0 Å among 65 pairs of Cα atoms aligned, and the BIgB

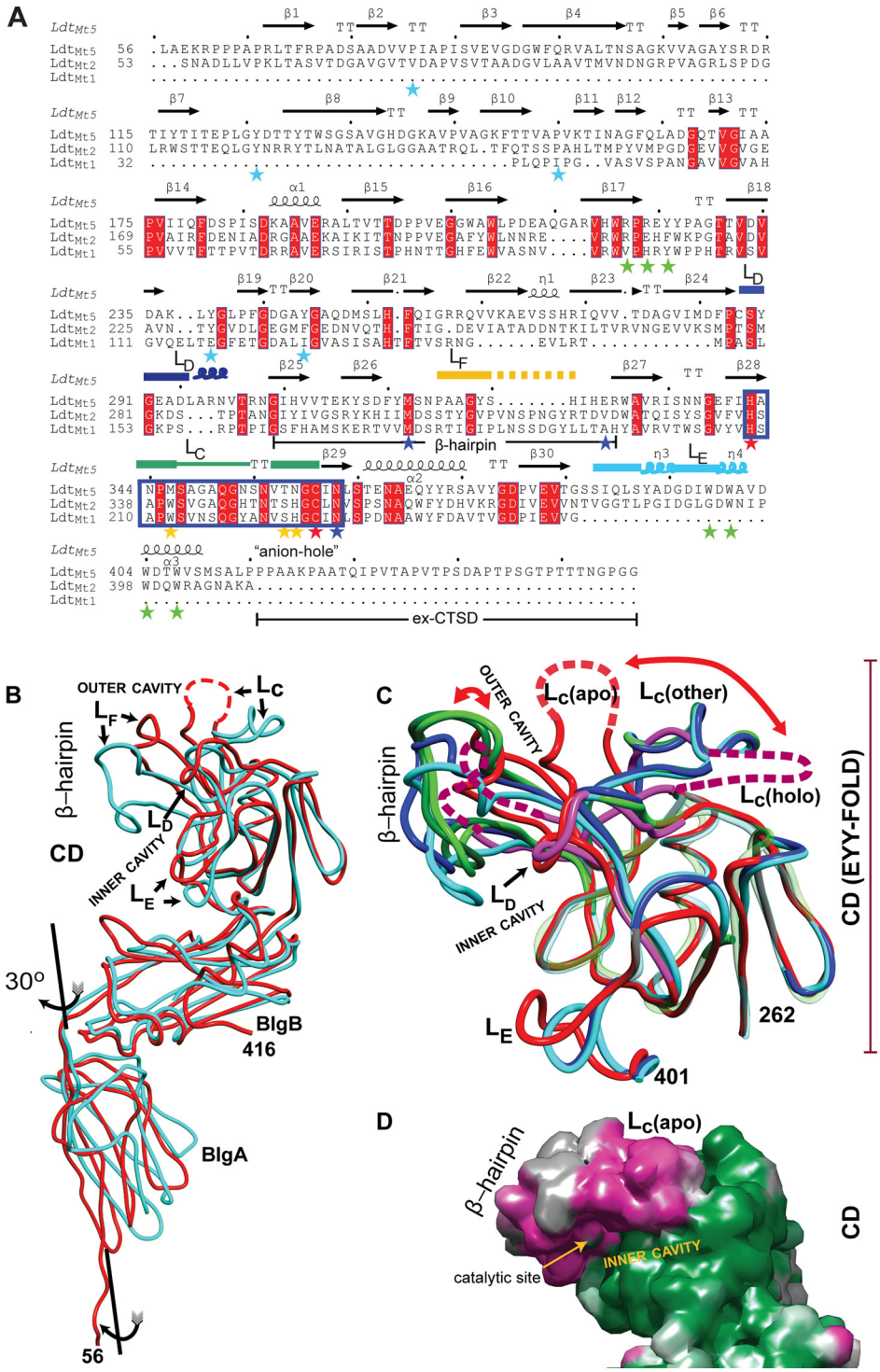

FIGURE 2. **Comparison of *M. tuberculosis* LD-transpeptidases.** *A*, the sequence alignment based on the structural superposition. The observed secondary structures are noted *above* the amino acid sequences. *Starred* residues are those highlighted in the text (*blue*, coordinating His^{342}; *cyan*, BlgA and BlgB interface; *green*, CTSD-BlgB-CD core interaction; *red*, catalytic residues; *yellow*, loop L_D). Named loops are also marked, and the characteristic LD-transpeptidase motif is *boxed* in *blue rectangle*. *B*, overlay of the apo structures of Ldt_{Mt2} (Protein Data Bank code 3VYN; in *cyan*) and Ldt_{Mt5} (this work; in *red*). Observed differences in the CD are concentrated in the β-hairpin and loops L_C–L_E. Disordered regions are represented as *dashed lines*. *C*, the Ldt_{Mt5} adduct structure displays the largest CD conformational changes among characterized LD-transpeptidases. The EYY-folded CD cores of apo-Ldt_{Mt5} (*red*), holo-Ldt_{Mt5} (*pink*), and the apo and holo crystal structures of Ldt_{Mt1} (Protein Data Bank code 4JMN, apo, in *light green*; Protein Data Bank code 4JMX, imipenem adduct, in *dark green*), and Ldt_{Mt2} (Protein Data Bank code 3VYN, apo, in *cyan*; Protein Data Bank code 3VYP, meropenem adduct, in *blue*) are shown as smoothed Cα traces. Structural elements with high r.m.s.d. are shown in *full opacity*; the remaining structural elements are displayed as *transparent* Cα traces to demonstrate conservation of the EYY-folded CD cores. The largest changes among structurally characterized LD-transpeptidases are observed in the β-hairpin, and in the case of Ldt_{Mt5}, there is a dramatic displacement of loop L_C that occurs after adduct formation (indicated with *red curved arrows*). The C-terminal portion of the CTSDs was excluded for clarity. *D*, accessible surface map of apo-Ldt_{Mt5} colored by the magnitude of the observed atomic temperature factors from low (*green*) to high (*magenta*) motility. The flexibility of the β-hairpin as indicated by the high atomic temperature factor correlates with its large displacement upon adduct formation. These images, the sequence alignment, and structural superpositions were performed using the program MOE. The sequence representation was performed using ESPript3 (48).

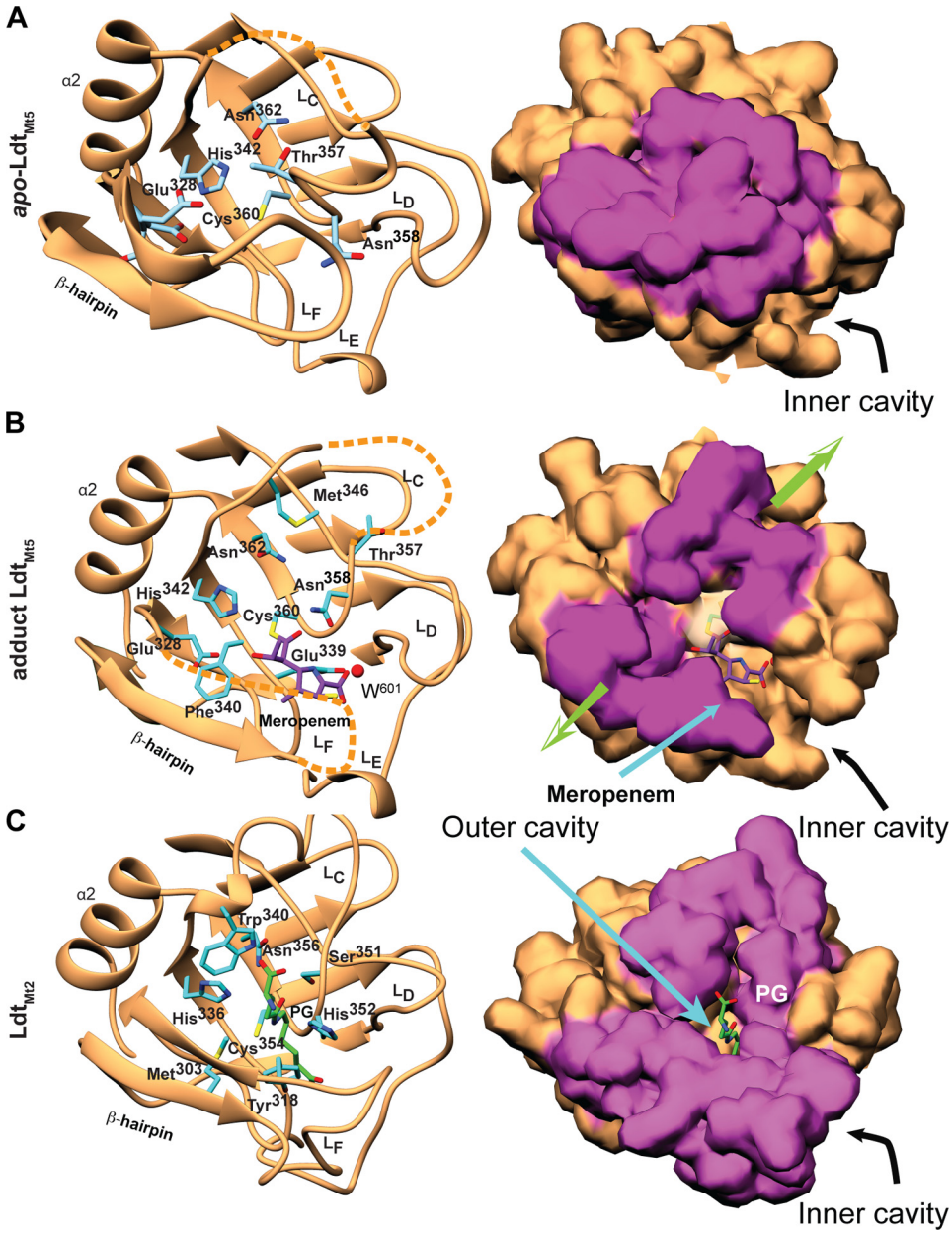

FIGURE 3. **Comparison of the Ldt_{Mt5} and Ldt_{Mt2} active sites.** *A*, apo-Ldt_{Mt5}; *B*, meropenem-bound Ldt_{Mt5} (meropenem adduct shown as *purple sticks*); *C*, Ldt_{Mt2}-PG fragment complex (Protein Data Bank code 3TUR; PG fragment shown as *cyan sticks*). The *left panels* show secondary structure schematic representations, and residues within the active site are represented as *sticks*. The *right panels* show the probe-accessible surface (3.5-Å radius). Surface zones related to the β-hairpin and loop L_C that display the largest structural differences among apo and holo structures are colored *purple*. Acylation of Ldt_{Mt5} by meropenem causes displacements of these structural elements as indicated by the *green arrows* (*right panel*) that "restore" the outer cavity.

domains display a r.m.s. deviation of 0.94 Å among 103 pairs of aligned Cα atoms. The EYY-folded CD cores of Ldt_{Mt1}, Ldt_{Mt2}, and Ldt_{Mt5} overlap well (Fig. 2*C*). However, differences localized to the β-hairpin flap (residues 312–330), loop L_C, and the C-terminal region of loop L_D increased the pairwise r.m.s.d. An r.m.s.d. of 1.25 Å for the 67 Cα atom pairs within the CD core was observed compared with r.m.s.d. values of 2.3 and 2.6 Å for 115 and 103 Cα atom pairs when the entire CD of Ldt_{Mt5} was compared with that of Ldt_{Mt2} and Ldt_{Mt1} (Protein Data Bank code 4JMN), respectively (the Ldt_{Mt1}/Ldt_{Mt2} overlap is 0.66 Å for 67 Cα atom pairs). Interestingly, the imipenem adduct structure of Ldt_{Mt1} (Protein Data Bank code 4JMX) minimally affects placement of the β-hairpin in comparison with its position in apo-Ldt_{Mt1}, whereas the meropenem adduct-Ldt_{Mt5} structure displays the largest changes in the β-hairpin (Fig. 2*C*).

The Conformation of the Ldt_{Mt5} BIg Domains Is Mostly Maintained by Unspecified Hydrophobic Interactions—A small, solvent-accessible area (312 Å^2) is buried in the interface between the BIg domains in Ldt_{Mt5}. A short, three-residue linker (Ala^{153}, Pro^{154}, and Val^{155}) joins BIgA and BIgB. BIgA is rotated ~30° around the axis passing through the interdomain linker compared with BIgA of Ldt_{Mt2} (Fig. 2*B*). Two hydrophobic patches comprising Pro^{80}, Tyr^{125}, and Pro^{154} of BIgA and Tyr^{239} and Tyr^{248} from BIgB and main-chain atoms of β-barrel loops from

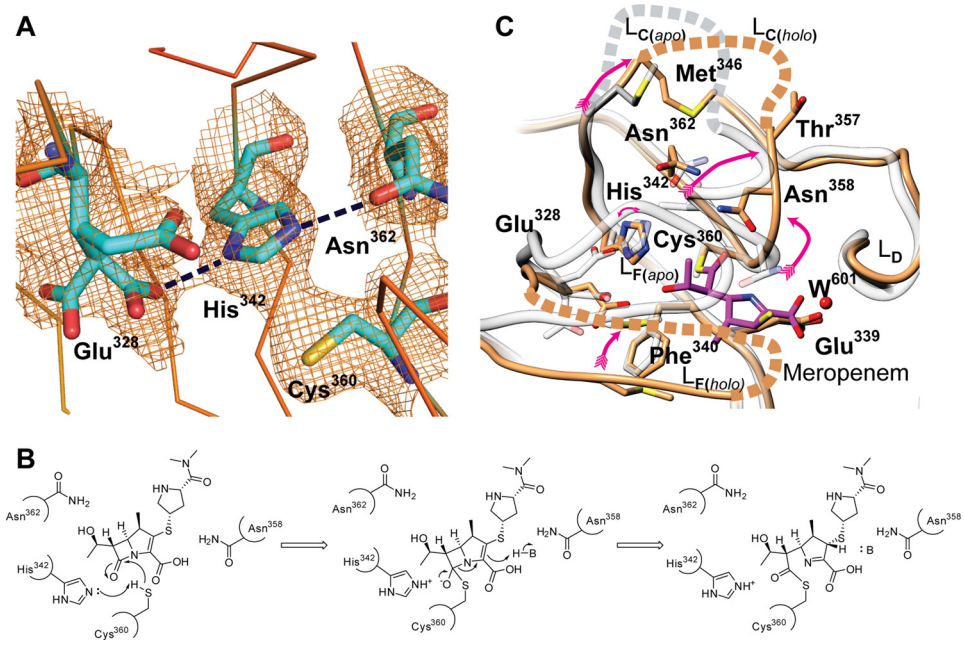

FIGURE 4. **An "active" conformation of Ldt_{Mt5} is achieved when meropenem binds.** *A*, a nonproductive orientation of His^{342} is observed in apo-Ldt_{Mt5} (σA-weighted electron density map contoured at 1.0 σ level). Residues of the refined structures are shown as *stick* representations. His^{342} is in close proximity to Cys^{360} as suggested by the electron density connecting these two residues. In addition, His^{342} hydrogen bonds with the most populated alternative conformation of Glu^{328} and Asn^{362} (*dashed lines*). Collectively, these interactions fix the imidazole ring in a nonproductive orientation that is not present in the meropenem adduct structure. *B*, mechanism of acylation of Ldt_{Mt5} by meropenem. *C*, overlay of active sites of apo and meropenem adduct structures. The *red arrows* indicate the large displacements of Met^{346} (Sδ–Sδ, 6.6 Å), Thr^{357} (Cβ–Cβ, 8.2 Å), and Asn^{358} (Cβ–Cβ, 4.1 Å) relative to the apo structure. The active site of apo-Ldt_{Mt5} is colored *gray*, and the meropenem adduct structure is colored *brown*. The ~180° rotation of His^{342} is noted with a *curved red arrow*. Meropenem is represented as *magenta sticks*. Disordered residues are represented as *dashed lines*. This figure was made using Chimera (19).

both of the domains make an interdomain contact. These proline and tyrosine residues are well conserved among three-domain LD-transpeptidases (Fig. 2*A*). Tyr^{125} (from BIgA) and Tyr^{239} (from BIgB) exchange hydrogen bonds with main-chain atoms of the opposite domain. This greasy and weak contact may provide flexibility in the orientation of the domains. In the Ldt_{Mt5} crystal form, a PEG molecule from the crystallization buffer is bound to an exposed hydrophobic patch (Pro^{122} and Tyr^{239}) at the interface of the BIgA and BIgB domains, apparently stabilizing the observed relative orientations of the domains.

The Conformations of the BIgB Domain and EYY-fold Are Maintained by the CTSD—The L_E loop of the Ldt_{Mt5} CTSD is slightly longer in comparison with that of Ldt_{Mt2} (Fig. 2, *B* and *C*). This loop wedges between the EYY-fold and the BIgB domain (Fig. 1). The Ldt_{Mt5} CTSD is rich in tryptophan residues (Trp^{398}, Trp^{400}, Trp^{404}, and Trp^{407}). Extensive hydrophobic contacts among the CTSD, BIgB, and CD domains increase the rigidity of the BIgB/CD assembly. In addition to regular contacts between Tyr^{392} and Trp^{398} in loop L_E with Leu^{209} and Pro^{210} in BIgB, the aromatic rings of Trp^{400}, Trp^{404}, and Trp^{407} in the α_3 helix of the CTSD form a "zipper-like" interaction with the aromatic ring of Tyr^{225} and aliphatic portions of the side chains of Arg^{223} and Arg^{221} of the BIgB domain. This structure provides 1336 $Å^2$ of additional area buried in the BIgB/EYY-fold assembly, which itself only contributes 433 $Å^2$.

The Ldt_{Mt5} CD Displays Large Structural Differences Relative to Ldt_{Mt1} and Ldt_{Mt2}—The CD of Ldt_{Mt5} displays marked differences in comparison with those of Ldt_{Mt1} and Ldt_{Mt2}. The largest differences are seen 1) within the fold and placement of a β-hairpin flap that includes loop L_F (the shortest among homologs), 2) in the conformation and partial disorder of loop L_C, and 3) in the size of loop L_D and loop L_E (of the CTSD) (Fig. 2). All of these structural differences are in close proximity to the Ldt_{Mt5} active site. The β-hairpin flap covers the active site and is the structural feature that distinguishes some LD-transpeptidases (10, 24, 28) from the first structurally characterized protein containing the EYY-fold (27). This flap displays the largest temperature factors relative to the remainder of Ldt_{Mt5} (Fig. 2*D*), is nine residues shorter in Ldt_{Mt5}, and displays low homology to other *M. tuberculosis* LD-transpeptidase β-hairpin flaps (Fig. 2*C*). In Ldt_{Mt5}, loop L_C displays considerable disorder. Electron density for residues 347–353 in apo-Ldt_{Mt5} and residues 348–356 in the meropenem adduct structure was not observed. However, the residues of loop L_C that are ordered display fold differences relative to Ldt_{Mt1} and Ldt_{Mt2} (Fig. 2*C*).

In previously solved LD-transpeptidase structures, the catalytic site is exposed through two connected cavities, the outer and inner cavities (Fig. 2, *B* and *C*). Compared with Ldt_{Mt1} and Ldt_{Mt2}, the small footprint and placement of this β-hairpin in Ldt_{Mt5} lead to greater exposure of the catalytic site from the inner cavity (Fig. 2). The β-hairpin flap and loop L_C of apo-Ldt_{Mt5} are shifted toward the outer cavity, closing it (Figs. 2*C* and 3*A*). In our meropenem adduct-Ldt_{Mt5} structure, the hairpin and loop are partially disordered; however, the ordered portions appear to shift away from the catalytic site, thereby exposing it (Fig. 3*B*). Thus, the acylation of Ldt_{Mt5} by meropenem

TABLE 3
Summary of mass spectrometry data obtained after preincubation of Ldt_{Mt5} and different carbapenems

Enzyme	Carbapenem	Calculated mass of inhibited species	Mass of carbapenem	Observed mass[a]
		Da	*Da*	*Da*
Ldt_{Mt5}	None	42,603		42,605
	Meropenem	42,986.5	383.5	42,605
	Imipenem	42,902.4	299.4	42,605
	Doripenem	43,023.1	420.1	42,604
	Biapenem	42,953.4	350.4	42,606
	Tebipenem	42,986.5	383.5	42,605
N358H/M346W Ldt_{Mt5}	None	42,681		42,683
	Meropenem	43,064.5	383.5	42,684
	Imipenem	42,980.4	299.4	42,683
	Doripenem	43,101.1	420.1	42,683
	Biapenem	43,031.4	350.4	42,683
	Tebipenem	43,064.5	383.5	42,684

[a] Reported masses are those that comprise the largest species in the mass spectrum at 100% abundance.

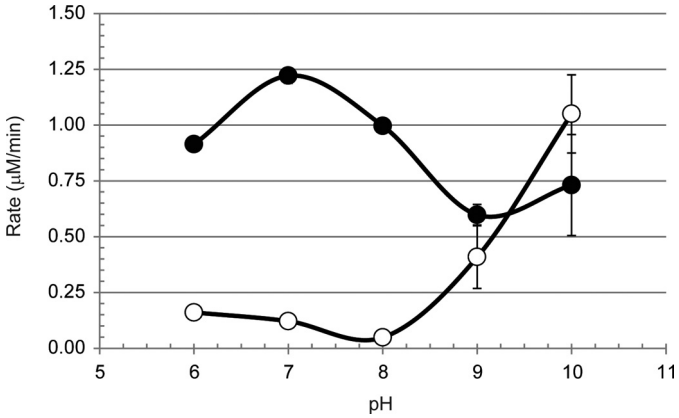

FIGURE 5. **pH rate profile analysis of Ldt_{Mt5} (*open circles*) and Ldt_{Mt2} (*closed circles*).** *Error bars* represent S.E.

TABLE 4
Summary of kinetic parameters for nitrocefin hydrolysis by Ldt_{Mt5} and Ldt_{Mt5} variants at pH 10
The Ldt_{Mt5} variants are listed in order of decreasing catalytic efficiency.

Enzyme	K_m	k_{cat}	k_{cat}/K_m
	μM	min^{-1}	$min^{-1}\cdot M^{-1}$
Ldt_{Mt5} N358H	50 ± 3	0.61 ± 0.03	$12.3 \pm 0.4 \times 10^3$
Ldt_{Mt5}	97 ± 19	0.79 ± 0.09	$8.7 \pm 1.9 \times 10^3$
Ldt_{Mt5} H342Q	151 ± 11	0.63 ± 0.01	$4.2 \pm 0.2 \times 10^3$
Ldt_{Mt5} H342A	153 ± 8	0.49 ± 0.01	$2.9 \pm 0.1 \times 10^3$
Ldt_{Mt5} T357V	262 ± 72	0.55 ± 0.08	$2.4 \pm 0.6 \times 10^3$
Ldt_{Mt5} N358A	125 ± 25	0.32 ± 0.02	$2.4 \pm 0.3 \times 10^3$
Ldt_{Mt5} N362A	175 ± 16	0.40 ± 0.01	$2.2 \pm 0.1 \times 10^3$
Ldt_{Mt5} C360A	211 ± 40	0.33 ± 0.02	$1.1 \pm 0.2 \times 10^3$

appears to "create" an outer cavity reminiscent of that observed in Ldt_{Mt1} and Ldt_{Mt2} (Fig. 3*C*).

Loop L_D (residues 289–302) within the CD core of Ldt_{Mt5} is larger compared with Loop L_D of Ldt_{Mt1} and Ldt_{Mt2} (Fig. 2*A*-C). The Ldt_{Mt5} L_D loop has a three-residue insertion that includes a bulky arginine residue (Arg^{297}) and forms a protruding insertion (Fig. 2*C*). Although most of this loop fold remains unperturbed, the insertion displaces the adjacent L_C loop (residues 338–358), thereby closing the active site outer cavity and dramatically modifying the fold and placement of the L_C loop.

The Ldt_{Mt5} Active Site Is Structurally Divergent Relative to Ldt_{Mt1} and Ldt_{Mt2}—The structural differences within the Ldt_{Mt5} CD have dramatic effects on the active site architecture and the readiness of catalytic residues to participate in enzymatic reactions and presumably PG stem recognition. In Ldt_{Mt1} and Ldt_{Mt2}, a conserved methionine residue (Met^{175} and Met^{303}, respectively) on the internal side of the β-hairpin flap limits the space around the catalytic cysteine. The unique placement of this loop in Ldt_{Mt5} results in displacement of this methionine (Met^{316} in Ldt_{Mt5}) by the non-conserved Glu^{328} (Fig. 3). Glu^{328} is substituted with smaller hydrophobic residues in Ldt_{Mt2} (Val^{322}) and Ldt_{Mt1} (Ala^{195}). Interestingly, the electron density surrounding this glutamate residue indicates that Glu^{328} is present in three alternative conformations in the apo-Ldt_{Mt5} structure but shows only one conformation in the meropenem adduct structure (Fig. 3, *A* and *B*). The most populated conformation of Glu^{328} and the conserved motif Asn^{362} (implicated in PG stem recognition) form hydrogen bonds with His^{342}, thereby orienting His^{342} in such a way that it is rotated 180° from the orientation required to deprotonate Cys^{360} (Fig. 4, *A* and *B*). Furthermore, Cys^{360} and His^{342} make a strong contact with one another; electron density connecting the sulfur atom to the imidazole ring carbon is visible in the experimental electron density map (Fig. 4*A*). However, no covalent bond is present: the coordination geometry of the Cϵ1–Sγ–Cβ bond angle is much smaller than 109°, which is expected for a direct bond. It is likely that this strong contact and coordination of the histidine ring by Asn^{362} and Glu^{328} make it difficult for the imidazole ring to rotate into a position that is better poised for catalysis (Fig. 4*B*). Thus, it is clear that His^{342} is not optimally poised to act as a catalytic base in Ldt_{Mt5} as is the equivalent residue in Ldt_{Mt2} (His^{336}) is (Fig. 3*C*).

The L_C loop of Ldt_{Mt5} is fully embedded in the conserved HXX_{14-17}(S/T)HGChN motif that characterizes this family of transpeptidases. Ldt_{Mt5} has two variations in the conserved motif: a motif alternative Thr^{357} of Ldt_{Mt5} replaces the Ldt_{Mt2} serine (Ser^{351}), and Asn^{358} replaces the characteristic motif histidine (His^{352} in Ldt_{Mt2}). The C-terminus of loop L_C forms the "anion hole" at the catalytic site of Ldt_{Mt2}. Thr^{357} occludes the outer entrance to the active site (Figs. 3*A* and 4*C*) where the PG stem binds to Ldt_{Mt2} (Fig. 3*C*) (10). The loop, which contains the anion hole that comprises a large quantity of positively charged atoms, is folded differently relative to Ldt_{Mt2}, and Met^{346} of loop L_C replaces a tryptophan residue that is conserved in all other *M. tuberculosis* LD-transpeptidases (Fig. 2*A*).

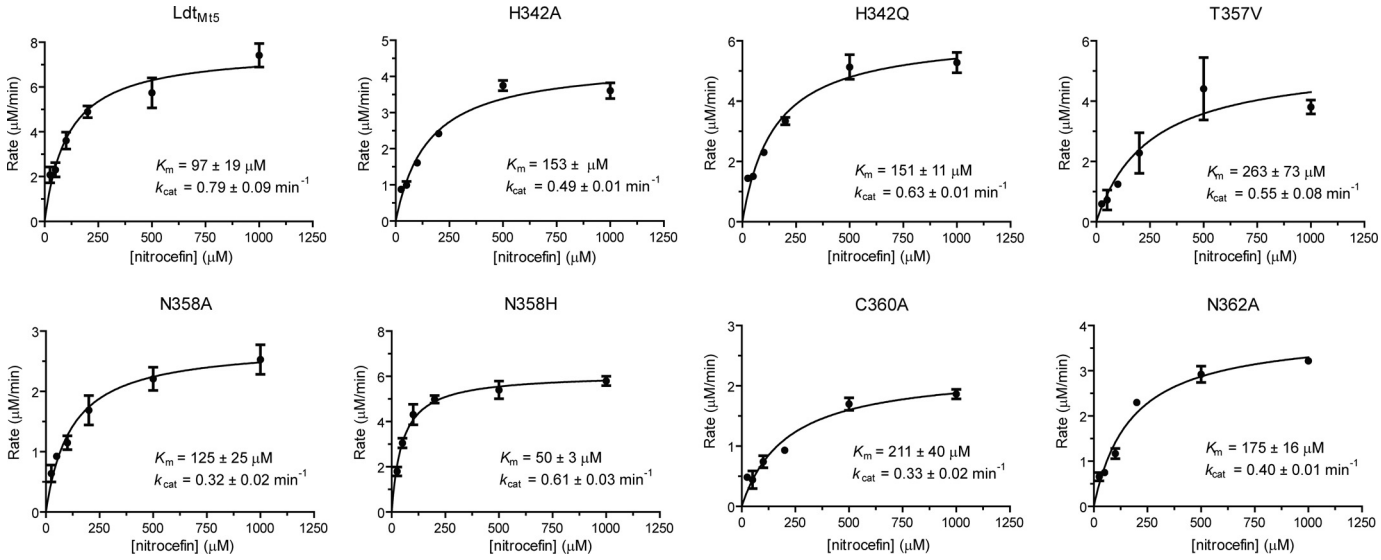

FIGURE 6. **Ldt_{Mt5} active site variants catalyze nitrocefin hydrolysis at pH 10.** Michaelis-Menten curves for Ldt_{Mt5} and Ldt_{Mt5} variants are shown. *Error bars* represent S.E.

Ldt_{Mt5} Is Acylated by Meropenem during Crystallization—The crystal form grown in the presence of meropenem shows electron density for Ldt_{Mt5} residues 56–317, 327–348, and 356–416. Electron density for most of the β-hairpin flap is missing in this crystal form, and like apo-Ldt_{Mt5}, most of loop L_C and the ex-CTSD are disordered. The carbapenem core of meropenem was fitted in additional electron density near the catalytic cysteine, which forms an adduct with Cys^{360} (Fig. 3*B*); however, no electron density for the 3-[5-(dimethylcarbamoyl)pyrrolidin-2-yl] group of meropenem was observed. Interestingly, the presence of this adduct restores the anion hole and other portions of L_C to a similar fold previously observed in other LD-transpeptidases, placing residues with a probable role in catalysis (Met^{346}, Asn^{358}, and Thr^{357}) in positions equivalent to those observed in active LD-transpeptidases (Fig. 4*C*). Thus, meropenem binding induces a conformational change that enables access to the catalytic site from the outer cavity as observed in other LD-transpeptidases (Fig. 3). In addition, this change promotes release of His^{342} from its nonproductive contact such that it now hydrogen bonds with Cys^{360} (distance of Nε–Sγ, 3.2 Å; Figs. 3*B* and 4*C*).

The most stable tautomer of the carbapenem core is observed where the ring nitrogen is deprotonated (double bond between C3 and N4) and C2 is sp^3 hybridized and is in agreement with previously reported Ldt_{Mt2}-meropenem adduct structures (24, 25). The meropenem core lies with its most apolar side facing a hydrophobic patch formed by Gly^{338}, the aliphatic portion of the side chain of Glu^{339}, and Phe^{340} at the inner cavity. The C-terminal portion of the main chain of loop L_C (Gly^{359}) provides apolar contacts with the other side of the carbapenem core. Four hydrophilic interactions are also observed between the carbapenem core and Ldt_{Mt5}: 1) Asn^{358} and 2) the main chain nitrogen atom of Cys^{360} hydrogen bond to the carbonyl of the opened penem ring, 3) Glu^{328} hydrogen bonds to the meropenem hydroxyethyl group, and 4) a water molecule (W^{601}) mediates interaction between the meropenem core carboxylate and the carboxylate of Glu^{339} (Fig. 3*B*).

We evaluated a series of β-lactams, including the carbapenems listed in Table 3, and measured the thermodynamics of β-lactam binding to Ldt_{Mt5} using ITC. Despite the presence of a meropenem adduct on Ldt_{Mt5}, no significant heat exchange associated with binding was measured by ITC, and no adduct was detected by mass spectrometry after a 5-h incubation of meropenem and Ldt_{Mt5} (Table 3).

Ldt_{Mt5}-catalyzed Nitrocefin Hydrolysis Is Optimal at Basic pH—Ldt_{Mt5} was probed for transpeptidase/β-lactamase activity using nitrocefin as a substrate. A pH rate profile analysis revealed that Ldt_{Mt5} is optimally active at pH >9 (Fig. 5) even after correcting for spontaneous ring opening at basic pH in the absence of enzyme, although its activity was not significantly different from that observed for Ldt_{Mt2}, which optimally catalyzes nitrocefin hydrolysis at pH 7 (10) (Fig. 5). We also measured nitrocefin binding at pH 8 where little Ldt_{Mt5}-catalyzed nitrocefin hydrolysis was observed (Fig. 5), but no detectable heat of exchange was observed using ITC (data not shown).

Conserved Active Site Residues Are Not Required for Nitrocefin Hydrolysis—On the basis of the apo-Ldt_{Mt5} structure, we rationally designed and purified Ldt_{Mt5} putative active site variants in an attempt to identify residues responsible for nitrocefin hydrolysis at pH >9. Surprisingly, all of the Ldt_{Mt5} variants evaluated, including C360A Ldt_{Mt5}, hydrolyzed nitrocefin (Table 4 and Fig. 6) with the rates of hydrolysis ordered as follows: N358H > wild type > H342Q > H342A > T357V > N358A > N362A > C360A. Although the rates of hydrolysis were relatively low, conservative mutations (N358H and H342Q) had the lowest impact on k_{cat}/K_m specificity constants, whereas C360A Ldt_{Mt5} was the least active variant we tested. Interestingly, the $K_{m(\text{nitrocefin})}$ for the N358H variant was 2-fold lower than that of wild type, whereas the k_{cat} values were relatively comparable.

Two residues at the ends of loop L_C that interact with the PG stem in the outer cavity of Ldt_{Mt2} (10), His^{352} and Trp^{340}, are substituted with Asn^{358} and Met^{346}, respectively, in Ldt_{Mt5}.

TABLE 5
Susceptibility of M. tuberculosis strains to isoniazid and carbapenems (and faropenem)
Values are reported as μg/ml.

Strain	Isoniazid	Ertapenem	Meropenem	Doripenem	Faropenem	Tebipenem pivoxil
Wild type	0.1	20	12.5	2.5	5	10
ldt_{Mt5}::Tn	0.1	20	12.5	1.2	2.5	10

Asn^{358} replaces this conserved motif histidine (His^{352}) in Ldt_{Mt2} that participates in recognition of the donor PG stem (10) and in Ldt_{Mt5} that participates in recognition of the meropenem adduct (Fig. 3*B*). Trp^{340} in Ldt_{Mt2} is proposed to provide tetrapeptide substrate specificity (10). In an attempt to make the Ldt_{Mt5} active site more Ldt_{Mt2}-like, we generated the Ldt_{Mt5} N358H/M346W double variant. Contrary to our expectations, mass spectrometry data indicate that the double variant was not acylated by the carbapenems tested (Table 3), and the double variant behaved like wild-type Ldt_{Mt5} when probed for its ability to catalyze nitrocefin hydrolysis in a pH rate profile analysis (data not shown).

Loss of ldt_{Mt5} Modestly Enhances Susceptibility to Doripenem and Faropenem—Recent studies have reported that, in addition to inhibiting DD-transpeptidase and carboxypeptidase activities, carbapenems and penems bind to and inhibit LD-transpeptidases (10, 24, 25, 29–31). We hypothesized that loss of Ldt_{Mt5} may alter sensitivity to carbapenems as the mutant lacking this protein would have one less target for carbapenems to inhibit. Minimum inhibitory concentration studies were performed to evaluate whether or not loss of ldt_{Mt5} affected the susceptibility of *M. tuberculosis* to carbapenems (Table 5). The ldt_{Mt5}::Tn strain reproducibly had modestly enhanced susceptibility to doripenem and faropenem (a penem) compared with wild type, but neither strain was susceptible to ertapenem or meropenem under the conditions that were tested. Both strains displayed similar susceptibilities to tebipenem pivoxil.

Mutations in the ldt_{Mt5} Locus Could Not be Detected in Meropenem-resistant Mutants—We tested the hypothesis that Ldt_{Mt5} is a target of meropenem and that meropenem-resistant *M. tuberculosis* strains would harbor a mutation in the gene encoding this enzyme. Toward this end, we generated genetically resistant strains by isolating mutants grown in the presence of 400 μg/ml meropenem. Nine independent strains were isolated, their genomic DNA was purified, and the ldt_{Mt5} loci (which included ~100 bp in both 5′- and 3′-UTRs) were PCR-amplified and sequenced. In addition, we sequenced the locus of the parent *M. tuberculosis* H37Rv that was used to generate the mutants. The DNA sequences of the ldt_{Mt5} loci in all nine meropenem-resistant strains were identical to the parent *M. tuberculosis* H37Rv and to the sequence of the reference *M. tuberculosis* H37Rv genome (data not shown) (32).

Loss of ldt_{Mt5} Enhances Sensitivity to Crystal Violet and Osmotic Shock—To determine the effects of loss of functional Ldt_{Mt5}, we probed the cell wall integrity of wild-type and ldt_{Mt5}::Tn strains using crystal violet and osmotic shock. In comparison with wild type, ldt_{Mt5}::Tn *M. tuberculosis* displayed a minor growth defect when grown in complete medium (Fig. 7*A*). When complete medium was supplemented with crystal violet, ldt_{Mt5}::Tn *M. tuberculosis* behaved similarly to cells lacking the dominant LD-transpeptidase Ldt_{Mt2} (ldt_{Mt2}::Tn) as both strains were more susceptible to killing by the dye (Fig. 7*B*). Furthermore, ldt_{Mt5}::Tn cells or ldt_{Mt2}::Tn cells were 2–3 times less viable than wild-type cells when subjected to osmotic challenge (Fig. 7*C*). These findings suggest that loss of ldt_{Mt5} alters

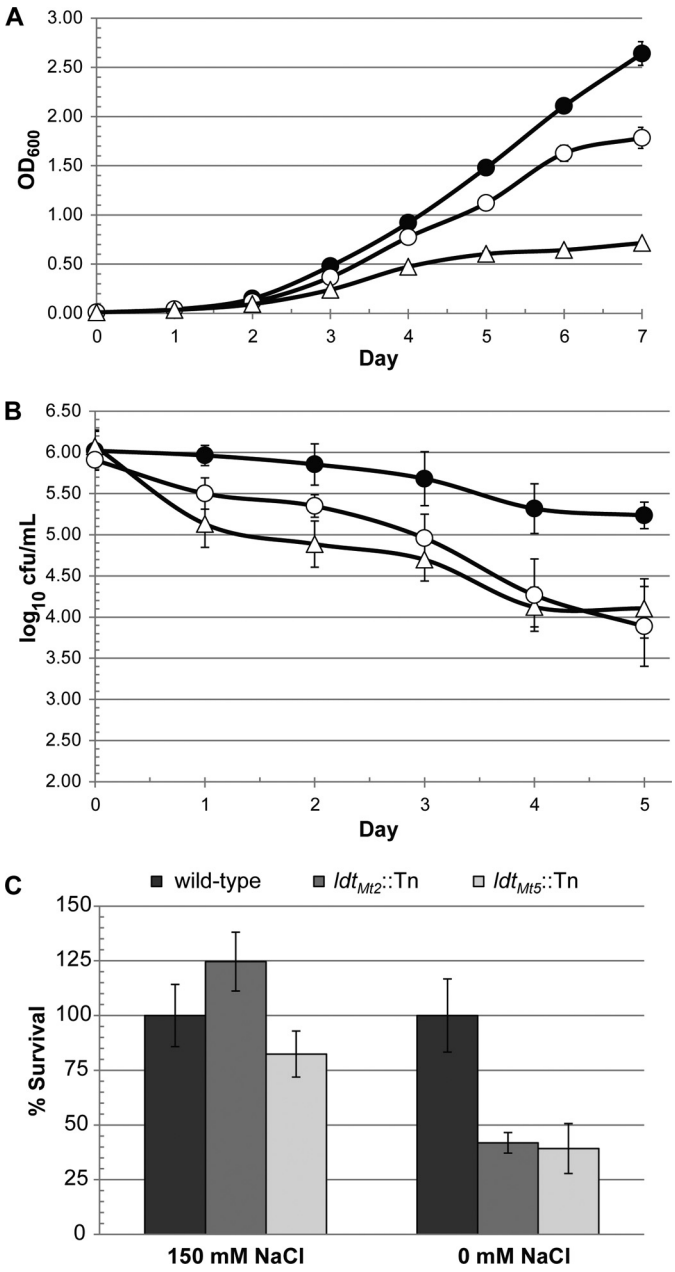

FIGURE 7. **Loss of Ldt_{Mt5} sensitizes *M. tuberculosis* to crystal violet and osmotic stress.** Wild-type (*closed circles*), ldt_{Mt5}::Tn (*open circles*), or ldt_{Mt2}::Tn (*triangles*) *M. tuberculosis* were grown in 7H9 complete medium (*A*) or 7H9 medium supplemented with crystal violet (*B*). *C*, strains lacking Ldt_{Mt2} or Ldt_{Mt5} are less tolerant to osmotic shock. *Error bars* represent S.E.

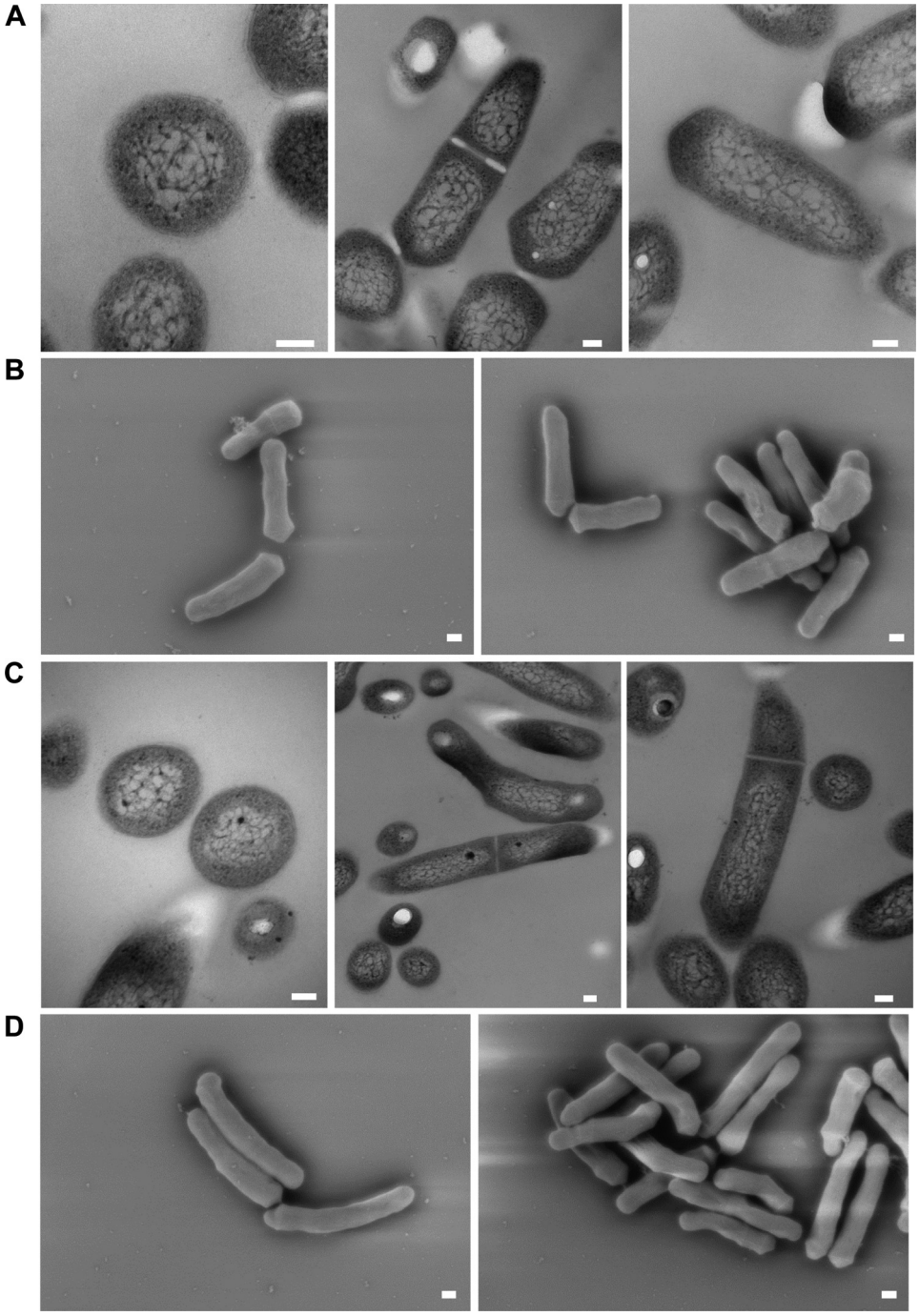

FIGURE 8. **Transmission (*A* and *C*) and scanning (*B* and *D*) electron microscopy reveals no significant changes in *M. tuberculosis* cell morphology upon loss of a functional copy of Ldt_{Mt5}.** *A* and *B*, wild-type *M. tuberculosis*; *C* and *D*, ldt_{Mt5}::Tn *M. tuberculosis*. *Scale bars* for transmission EM images (*A* and *C*) and scanning EM images (*B* and *C*) represent 100 and 200 nm, respectively.

cell wall permeability and sensitivity to crystal violet and compromises cell wall integrity. We also examined the cell morphology of *M. tuberculosis* lacking ldt_{Mt5} by electron microscopy. Interestingly, no observable changes in cell size and morphology between wild-type and ldt_{Mt5}::Tn strains were observed (Fig. 8). The gene encoding Ldt_{Mt5} is in an operon downstream of *murB*, another PG biosynthetic enzyme. We attempted to complement our ldt_{Mt5}::Tn strain with a wild-type copy of ldt_{Mt5} under the control of its native promoter. We designed and tested eight different complemented strains, but none were able to restore growth phenotypes (data not shown).

Discussion

Recently, 3→3 cross-links have been identified in the PG of a variety of bacterial species (5, 33–36), and LD-transpeptidases have been identified as the enzymes that catalyze synthesis of this type of transpeptide bond (6–8, 12, 33, 37, 38). Ldt_{Mt5} is a paralog of Ldt_{Mt2} from *M. tuberculosis* and has been reported to

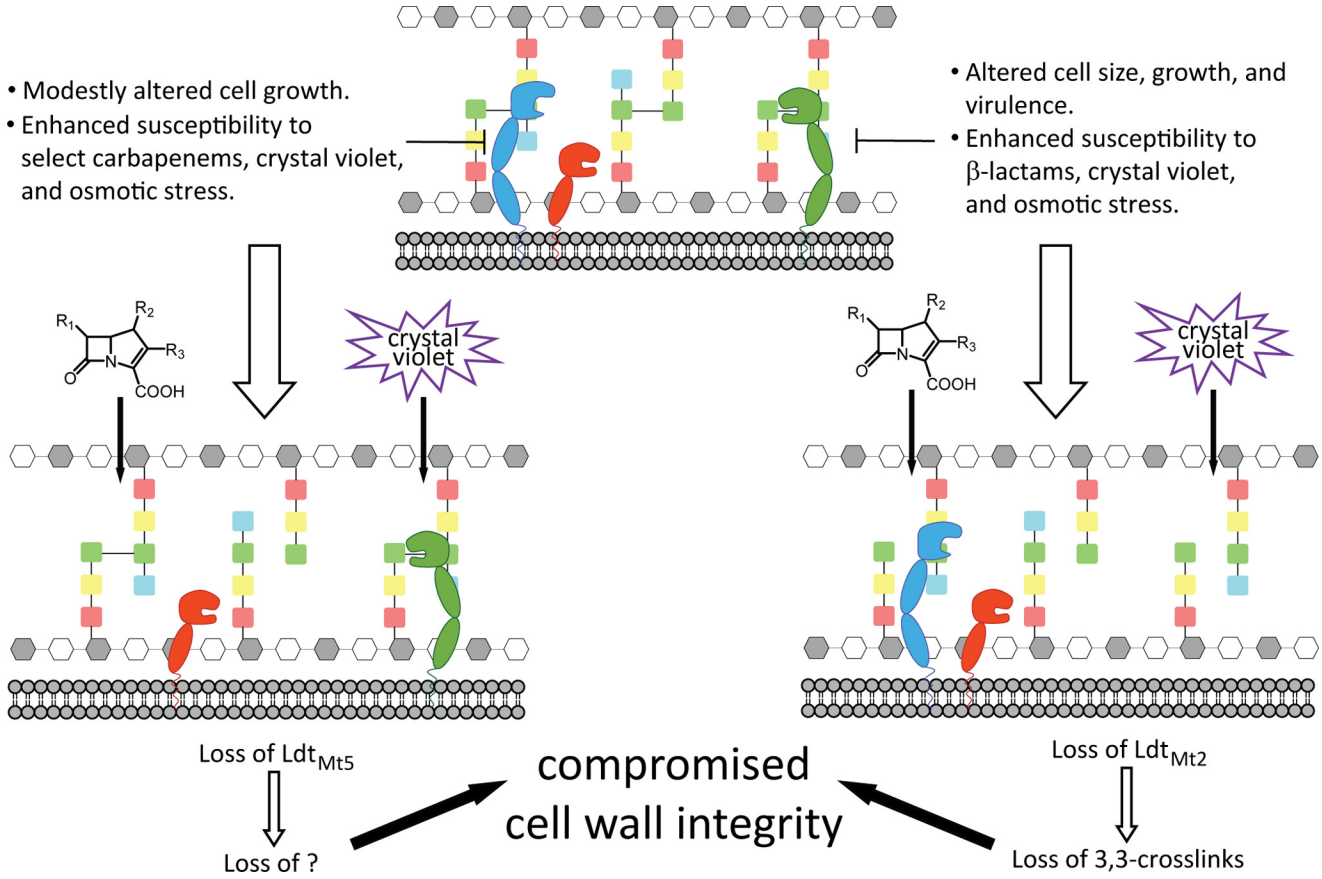

FIGURE 9. **Loss of Ldt_{Mt2} or Ldt_{Mt5} compromises *M. tuberculosis* cell wall integrity.** The *M. tuberculosis* PG is 3→3 and 4→3 cross-linked by LD- and DD-transpeptidases (not shown), respectively. Both Ldt_{Mt2} (*green*) and Ldt_{Mt5} (*blue*) have two Blg domains, whereas Ldt_{Mt1} (*red*) has one, which likely differentially positions the LD-transpeptidases within the periplasm. Although loss of Ldt_{Mt1} alone results in no discernible phenotype, loss of Ldt_{Mt2} results in compromised cell wall integrity as a result of loss of 3→3 cross-links in PG. Ldt_{Mt5} has a structurally distinct active site relative to both Ldt_{Mt1} and Ldt_{Mt2}, and when Ldt_{Mt5} is lost, *M. tuberculosis* is sensitized to chemical probes and osmotic stress similarly to when Ldt_{Mt2} is lost. Although Ldt_{Mt5} can catalyze 3→3 cross-link formation *in vitro*, its physiological function remains unclear.

catalyze formation of 3→3 transpeptide linkages in PG substrates derived from *Mycobacterium abscessus* (30).

There are significant structural differences within the CD of Ldt_{Mt5} and consequently the active site despite overall architectural similarity to Ldt_{Mt2}. The β-hairpin flap that covers the active site is the smallest among paralogs and exhibits high mobility (high B factors in the apo structure and partial disorder observed in the meropenem-bound structure; Fig. 2*D*). This hairpin and loop L_C display the largest structural differences among *M. tuberculosis* LD-transpeptidases (Fig. 2*A*), and the distinctive structural changes observed upon meropenem adduct formation suggest that their mobility and flexibility could play a role in the catalytic mechanism. The outer cavity that is present in other characterized LD-transpeptidases is absent in apo-Ldt_{Mt5}; however, such an outer cavity is restored when meropenem acylates Ldt_{Mt5}. Upon acylation by meropenem, residues from the conserved motif, including His^{342}, Asn^{358}, Cys^{360}, and Asn^{362}, shift to positions resembling those occupied by equivalent residues in Ldt_{Mt2} (Figs. 3, *B* and *C*, and 4*A*) and Ldt_{Mt1}, lining a cavity that could accommodate a PG stem (Fig. 3).

We observed catalytic residues Cys^{360} and His^{342} in a nonproductive contact in our apo crystal form, and His^{342} is not optimally poised for catalysis (Fig. 4*A*); however, the nonproductive contact appears to be released upon adduct formation (Fig. 4*B*). We did not observe acylated Ldt_{Mt5} by mass spectrometry, likely the result of the presence of this nonproductive contact. However, we clearly observed a meropenem adduct on Ldt_{Mt5} in our crystal form. Thus, if given enough time, meropenem will acylate Ldt_{Mt5} over the extended incubation period that is required for co-crystallization. Alternatively, a component of the crystallization buffer may promote acylation of Ldt_{Mt5} by meropenem.

The pK_a of a cysteine side chain is 8.3. Nitrocefin is a poor substrate for Ldt_{Mt5}, but we observed Ldt_{Mt5}-catalyzed nitrocefin hydrolysis at pH >9 (Fig. 5). It is feasible that the nonproductive contact of the catalytic residues may be released at pH ≥9 by weakening of the hydrogen bonds holding the residues in this conformation (Fig. 4*A*). None of the active site variants we designed fully abolished this activity, including C360A Ldt_{Mt5}; however,C360A Ldt_{Mt5} was the least active variant. Furthermore, the N358H substitution affected nitrocefin recognition ($K_m^{N358H} < K_m^{WT}$). It has been demonstrated previously that substitutions to any of the catalytic residues of serine proteases significantly reduce the rate of peptide bond cleavage but do not completely abolish it (39), indicating that the remaining catalytic site environment after residue substitutions can still promote turn-

over albeit slowly. It is feasible that, under basic conditions, Cys^{360} is deprotonated and can hydrolyze nitrocefin and that excess hydroxide in the Ldt_{Mt5} active site will still promote turnover of this unnatural substrate even in the absence of the catalytic cysteine. Alternatively, different Ldt_{Mt5} residues may mediate nitrocefin hydrolysis.

In addition to catalyzing 3→3 transpeptidation in PG, LD-transpeptidases incorporate non-canonical D-amino acids into PG during stationary growth phase and catalyze attachment of Braun lipoprotein in some Gram-negative bacteria (12, 40). Unlike Ldt_{Mt2}, Ldt_{Mt5} has a 33-residue ex-CTSD (residues 417–451). The ex-CTSD (Fig. 1) is disordered and contains proline-rich stretches (Fig. 2*A*). Proline-rich regions have been observed in other mycobacterial PG biosynthetic enzymes, including putative DD-transpeptidases PonA1, PonA2, and PonA3 and Ldt_{Mt4}, another paralog of Ldt_{Mt2} (41, 42). Although these proline-rich regions are seemingly common among these *M. tuberculosis* cell wall biosynthetic enzymes, their role in *M. tuberculosis* physiology is still largely unknown. Interestingly, proline-rich sequence stretches frequently mediate protein-protein interactions (43). The proline-rich ex-CTSD of Ldt_{Mt5} is in close proximity to the catalytic site. Thus, it is plausible that the Ldt_{Mt5} ex-CTSD participates in the recognition of protein substrates and/or binding partners, and these interactions may drive the conformational changes required to release His^{342} and Cys^{360} from their nonproductive contact. Likewise, it is reasonable to speculate that the active site of Ldt_{Mt5} may have evolved to accommodate large substrates like proteins and play a role in anchoring them to the PG reminiscent of the role LD-transpeptidases serve in Gram-negative species in anchoring Braun lipoprotein (12, 40). Taken together, the major structural differences and divergent catalytic site suggest that Ldt_{Mt5} and Ldt_{Mt2} evolved to serve different functions in *M. tuberculosis* (Fig. 9).

It has been demonstrated that YbiS, an *E. coli* LD-transpeptidase, is a substrate of the thioreductase DsbG (44). In *E. coli*, DsbG reduces the catalytic cysteine of YbiS that is prone to sulfenylation in the periplasm. We have previously reported a crystal structure of Ldt_{Mt2} that shows Cys^{354} oxidized to the sulfenic acid (10), suggesting that *M. tuberculosis* LD-transpeptidases are also susceptible to oxidation. Although we did not observe any sulfur adducts in our apo-Ldt_{Mt5} structure, it is conceivable that Ldt_{Mt5} requires binding of a protein partner to maintain the correct oxidation state of its catalytic cysteine *in vivo*.

Although all β-lactam antibiotics target DD-transpeptidases involved in 4→3 cross-link formation in PG maturation, only the carbapenem class of β-lactams (and faropenem, a penem) inhibit LD-transpeptidases. Furthermore, the genome of *M. tuberculosis* encodes for BlaC, an extended spectrum class A β-lactamase (45, 46). For these historical reasons, β-lactams are seldom considered for treatment of *M. tuberculosis* infection. However, carbapenems have been recently identified as poor substrates for BlaC (47). We have previously demonstrated that *M. tuberculosis* lacking Ldt_{Mt2} is more susceptible to killing by β-lactams (8, 14). Sanders *et al.* (42) have reported that LdtC (homologous to Ldt_{Mt5} in *M. tuberculosis* on the basis of sequence) is the primary LD-transpeptidase in *Mycobacterium smegmatis*. Strains lacking *ldtC* are hypersusceptible to imipenem, and ldt_{Mt5} from *M tuberculosis* fully complements this phenotype in an *ldtC* mutant, suggesting that these enzymes are equivalent (42). We observed a modest enhancement in susceptibility of the ldt_{Mt5}::Tn strain to select carbapenems (Table 5) presumably due to synthetic lethality as these β-lactams may inactivate other targets. Although our meropenem adduct crystal form supported very slow acylation of Ldt_{Mt5} over many days, we cannot rule out the possibility that Ldt_{Mt5} was more rapidly inactivated by this class of β-lactams *in vivo*, particularly in the event that Ldt_{Mt5} requires a protein-protein interaction for productive catalysis. To date, studies examining acylation of Ldt_{Mt5} by carbapenems, including the data presented here, have been *in vitro*, and interestingly, Ldt_{Mt5} is the only Ldt_{Mt2} paralog that is not inactivated by carbapenems. The increased susceptibility of ldt_{Mt5}::Tn strains to osmotic shock and crystal violet coupled with the observed modest enhancement in susceptibility to carbapenems and our meropenem-Ldt_{Mt5} crystal form suggest that Ldt_{Mt5} is worth pursuing as a drug target.

Author Contributions—L. A. B. B. and G. L. conceived the study, and L. A. B. B., G. L., and M. A. B. designed the study. L. A. B. B. and G. L. designed and performed the biochemical and genetic experiments and analyzed the results. L. A. B. B. prepared all proteins and together with A. G. and M. A. B. performed the crystallization experiments and preliminary crystal quality analysis; J. J. collected the crystallographic data at synchrotron facilities. A. G. and M. A. B. carried out the crystallographic and structural analyses. Y. P. and M. A. B. performed the ITC experiments. L. A. B. B. and G. L. prepared samples for mass spectrometry, and E. P. L. and C. A. T. performed and analyzed the mass spectrometry data. L. A. B. B., G. L., and M. A. B. wrote the manuscript. All authors reviewed the results and approved the final version of the manuscript.

Acknowledgment—We kindly thank Amit Kaushik for assistance with genetic experiments and Maia Schoonmaker Arnold and Mike Delanoy for assistance with electron microscopy. Research was carried out at X6A beamline funded by the National Institute of General Medical Sciences, National Institute of Health under Agreement GM-0080. The National Synchrotron Light Source, Brookhaven National Laboratory is supported by the United States Department of Energy under Contract DE-AC02-98CH10886.

References

1. Walsh, C. (2003) *Antibiotics: Actions, Origins, Resistance*, ASM Press, Washington, D. C.
2. Cho, H., Uehara, T., and Bernhardt, T. (2014) β-Lactam antibiotics induce a lethal malfunctioning of the bacterial cell wall synthesis machinery. *Cell* **159,** 1300–1311
3. Meroueh, S. O., Bencze, K. Z., Hesek, D., Lee, M., Fisher, J. F., Stemmler, T. L., and Mobashery, S. (2006) Three-dimensional structure of the bacterial cell wall peptidoglycan. *Proc. Natl. Acad. Sci. U.S.A.* **103,** 4404–4409
4. Lamichhane, G., Freundlich, J. S., Ekins, S., Wickramaratne, N., Nolan, S. T., and Bishai, W. R. (2011) Essential metabolites of *Mycobacterium tuberculosis* and their mimics. *mBio* **2,** e00301–10
5. Wietzerbin, J., Das, B. C., Petit, J. F., Lederer, E., Leyh-Bouille, M., and Ghuysen, J. M. (1974) Occurrence of D-alanyl-(D)-*meso*-diaminopimelic acid and *meso*-diaminopimelyl-*meso*-diaminopimelic acid interpeptide linkages in the peptidoglycan of mycobacteria. *Biochemistry* **13,**

3471–3476
6. Lavollay, M., Arthur, M., Fourgeaud, M., Dubost, L., Marie, A., Veziris, N., Blanot, D., Gutmann, L., and Mainardi, J. (2008) The peptidoglycan of stationary-phase *Mycobacterium tuberculosis* predominantly contains cross-links generated by L,D-transpeptidation. *J. Bacteriol.* **190,** 4360–4366
7. Lavollay, M., Fourgeaud, M., Herrmann, J. L., Dubost, L., Marie, A., Gutmann, L., Arthur, M., and Mainardi, J. L. (2011) The peptidoglycan of *Mycobacterium abscessus* is predominantly cross-linked by L,D-transpeptidases. *J. Bacteriol.* **193,** 778–782
8. Gupta, R., Lavollay, M., Mainardi, J. L., Arthur, M., Bishai, W. R., and Lamichhane, G. (2010) The *Mycobacterium tuberculosis* protein Ldt_{Mt2} is a nonclassical transpeptidase required for virulence and resistance to amoxicillin. *Nat. Med.* **16,** 466–469
9. Ghuysen, J. M. (1991) Serine β-lactamases and penicillin-binding proteins. *Annu. Rev. Microbiol.* **45,** 37–67
10. Erdemli, S. B., Gupta, R., Bishai, W. R., Lamichhane, G., Amzel, L. M., and Bianchet, M. A. (2012) Targeting the cell wall of *Mycobacterium tuberculosis*: structure and mechanism of L,D-transpeptidase 2. *Structure* **20,** 2103–2115
11. Mainardi, J. L., Fourgeaud, M., Hugonnet, J. E., Dubost, L., Brouard, J. P., Ouazzani, J., Rice, L. B., Gutmann, L., and Arthur, M. (2005) A novel peptidoglycan cross-linking enzyme for a β-lactam-resistant transpeptidation pathway. *J. Biol. Chem.* **280,** 38146–38152
12. Magnet, S., Dubost, L., Marie, A., Arthur, M., and Gutmann, L. (2008) Identification of the L,D-transpeptidases for peptidoglycan cross-linking in *Escherichia coli*. *J. Bacteriol.* **190,** 4782–4785
13. Sanders, A. N., and Pavelka, M. S. (2013) Phenotypic analysis of *Escherichia coli* mutants lacking L,D-transpeptidases. *Microbiology* **159,** 1842–1852
14. Schoonmaker, M. K., Bishai, W. R., and Lamichhane, G. (2014) Nonclassical transpeptidases of *Mycobacterium tuberculosis* alter cell size, morphology, the cytosolic matrix, protein localization, virulence, and resistance to β-lactams. *J. Bacteriol.* **196,** 1394–1402
15. Edelheit, O., Hanukoglu, A., and Hanukoglu, I. (2009) Simple and efficient site-directed mutagenesis using two single-primer reactions in parallel to generate mutants for protein structure-function studies. *BMC Biotechnol.* **9,** 61
16. Winn, M. D., Ballard, C. C., Cowtan, K. D., Dodson, E. J., Emsley, P., Evans, P. R., Keegan, R. M., Krissinel, E. B., Leslie, A. G., McCoy, A., McNicholas, S. J., Murshudov, G. N., Pannu, N. S., Potterton, E. A., Powell, H. R., Read, R. J., Vagin, A., and Wilson, K. S. (2011) Overview of the CCP4 suite and current developments. *Acta Crystallogr. D Biol. Crystallogr.* **67,** 235–242
17. Emsley, P., Lohkamp, B., Scott, W. G., and Cowtan, K. (2010) Features and development of Coot. *Acta Crystallogr. D Biol. Crystallogr.* **66,** 486–501
18. Adams, P. D., Afonine, P. V., Bunkóczi, G., Chen, V. B., Davis, I. W., Echols, N., Headd, J. J., Hung, L. W., Kapral, G. J., Grosse-Kunstleve, R. W., McCoy, A. J., Moriarty, N. W., Oeffner, R., Read, R. J., Richardson, D. C., Richardson, J. S., Terwilliger, T. C., and Zwart, P. H. (2010) PHENIX: a comprehensive python-based system for macromolecular structure solution. *Acta Crystallogr. D Biol. Crystallogr.* **66,** 213–221
19. Pettersen, E. F., Goddard, T. D., Huang, C. C., Couch, G. S., Greenblatt, D. M., Meng, E. C., and Ferrin, T. E. (2004) UCSF Chimera—a visualization system for exploratory research and analysis. *J. Comput. Chem.* **25,** 1605–1612
20. Krissinel, E., and Henrick, K. (2007) Inference of macromolecular assemblies from crystalline state. *J. Mol. Biol.* **372,** 774–797
21. Valway, S. E., Sanchez, M. P., Shinnick, T. F., Orme, I., Agerton, T., Hoy, D., Jones, J. S., Westmoreland, H., and Onorato, I. M. (1998) An outbreak involving extensive transmission of a virulent strain of *Mycobacterium tuberculosis*. *N. Engl. J. Med.* **338,** 633–639
22. Lamichhane, G., Zignol, M., Blades, N. J., Geiman, D. E., Dougherty, A., Grosset, J., Broman, K. W., and Bishai, W. R. (2003) A postgenomic method for predicting essential genes at subsaturation levels of mutagenesis: application to *Mycobacterium tuberculosis*. *Proc. Natl. Acad. Sci. U.S.A.* **100,** 7213–7218
23. Cynamon, M. H., Speirs, R. J., and Welch, J. T. (1998) *In vitro* antimycobacterial activity of 5-chloropyrazinamide. *Antimicrob. Agents. Chemother.* **42,** 462–463
24. Kim, H. S., Kim, J., Im, H. N., Yoon, J. Y., An, D. R., Yoon, H. J., Kim, J. Y., Min, H. K., Kim, S. J., Lee, J. Y., Han, B. W., and Suh, S. W. (2013) Structural basis for the inhibition of *Mycobacterium tuberculosis* L,D-transpeptidase by meropenem, a drug effective against extensively drug-resistant strains. *Acta Crystallogr. D Biol. Crystallogr.* **69,** 420–431
25. Li, W. J., Li, D. F., Hu, Y. L., Zhang, X. E., Bi, L. J., and Wang, D. C. (2013) Crystal structure of L,D-transpeptidase Ldt_{Mt2} in complex with meropenem reveals the mechanism of carbapenem against *Mycobacterium tuberculosis*. *Cell Res.* **23,** 728–731
26. Böth, D., Steiner, E. M., Stadler, D., Lindqvist, Y., Schnell, R., and Schneider, G. (2013) Structure of Ldt_{Mt2}, an L,D-transpeptidase from *Mycobacterium tuberculosis*. *Acta Crystallogr. D Biol. Crystallogr.* **69,** 432–441
27. Bielnicki, J., Devedjiev, Y., Derewenda, U., Dauter, Z., Joachimiak, A., and Derewenda, Z. S. (2006) *B. subtilis* ykuD protein at 2.0 Å resolution: insights into the structure and function of a novel, ubiquitous family of bacterial enzymes. *Proteins* **62,** 144–151
28. Biarrotte-Sorin, S., Hugonnet, J. E., Delfosse, V., Mainardi, J. L., Gutmann, L., Arthur, M., and Mayer, C. (2006) Crystal structure of a novel β-lactam-insensitive peptidoglycan transpeptidase. *J. Mol. Biol.* **359,** 533–538
29. Correale, S., Ruggiero, A., Capparelli, R., Pedone, E., and Berisio, R. (2013) Structures of free and inhibited forms of the L,D-transpeptidase Ldt_{Mt1} from *Mycobacterium tuberculosis*. *Acta Crystallogr. D Biol. Crystallogr.* **69,** 1697–1706
30. Cordillot, M., Dubée, V., Triboulet, S., Dubost, L., Marie, A., Hugonnet, J. E., Arthur, M., and Mainardi, J. L. (2013) *In vitro* cross-linking of *Mycobacterium tuberculosis* peptidoglycan by L,D-transpeptidases and inactivation of these enzymes by carbapenems. *Antimicrob. Agents Chemother.* **57,** 5940–5945
31. Kumar, P., Arora, K., Lloyd, J. R., Lee, I. Y., Nair, V., Fischer, E., Boshoff, H. I., and Barry, C. E., 3rd (2012) Meropenem inhibits D,D-carboxypeptidase activity in *Mycobacterium tuberculosis*. *Mol. Microbiol.* **86,** 367–381
32. Cole, S. T., Brosch, R., Parkhill, J., Garnier, T., Churcher, C., Harris, D., Gordon, S. V., Eiglmeier, K., Gas, S., Barry, C. E., 3rd, Tekaia, F., Badcock, K., Basham, D., Brown, D., Chillingworth, T., Connor, R., Davies, R., Devlin, K., Feltwell, T., Gentles, S., Hamlin, N., Holroyd, S., Hornsby, T., Jagels, K., Krogh, A., McLean, J., Moule, S., Murphy, L., Oliver, K., Osborne, J., Quail, M. A., Rajandream, M. A., Rogers, J., Rutter, S., Seeger, K., Skelton, J., Squares, R., Squares, S., Sulston, J. E., Taylor, K., Whitehead, S., and Barrell, B. G. (1998) Deciphering the biology of *Mycobacterium tuberculosis* from the complete genome sequence. *Nature* **393,** 537–544
33. Mainardi, J. L., Morel, V., Fourgeaud, M., Cremniter, J., Blanot, D., Legrand, R., Frehel, C., Arthur, M., Van Heijenoort, J., and Gutmann, L. (2002) Balance between two transpeptidation mechanisms determines the expression of β-lactam resistance in *Enterococcus faecium*. *J. Biol. Chem.* **277,** 35801–35807
34. Pisabarro, A. G., de Pedro, M. A., and Vázquez, D. (1985) Structural modifications in the peptidoglycan of *Escherichia coli* associated with changes in the state of growth of the culture. *J. Bacteriol.* **161,** 238–242
35. Peltier, J., Courtin, P., El Meouche, I., Lemée, L., Chapot-Chartier, M. P., and Pons, J. L. (2011) *Clostridium difficile* has an original peptidoglycan structure with a high level of *N*-acetylglucosamine deacetylation and mainly 3-3 cross-links. *J. Biol. Chem.* **286,** 29053–29062
36. Hugonnet, J. E., Haddache, N., Veckerlé, C., Dubost, L., Marie, A., Shikura, N., Mainardi, J. L., Rice, L. B., and Arthur, M. (2014) Peptidoglycan cross-linking in glycopeptide-resistant Actinomycetales. *Antimicrob. Agents Chemother.* **58,** 1749–1756
37. Magnet, S., Arbeloa, A., Mainardi, J. L., Hugonnet, J. E., Fourgeaud, M., Dubost, L., Marie, A., Delfosse, V., Mayer, C., Rice, L. B., and Arthur, M. (2007) Specificity of L,D-transpeptidases from Gram-positive bacteria producing different peptidoglycan chemotypes. *J. Biol. Chem.* **282,** 13151–13159
38. Cava, F., de Pedro, M. A., Lam, H., Davis, B. M., and Waldor, M. K. (2011) Distinct pathways for modification of the bacterial cell wall by non-canonical D-amino acids. *EMBO J.* **30,** 3442–3453
39. Corey, D. R., and Craik, C. S. (1992) An investigation into the minimum requirements for peptide hydrolysis by mutation of the catalytic triad of trypsin. *J. Am. Chem. Soc.* **114,** 1784–1790

40. Magnet, S., Bellais, S., Dubost, L., Fourgeaud, M., Mainardi, J. L., Petit-Frère, S., Marie, A., Mengin-Lecreulx, D., Arthur, M., and Gutmann, L. (2007) Identification of the L,D-transpeptidases responsible for attachment of the Braun lipoprotein to *Escherichia coli* peptidoglycan. *J. Bacteriol.* **189,** 3927–3931
41. Patru, M. M., and Pavelka, M. S., Jr. (2010) A role for the class A penicillin-binding protein PonA2 in the survival of *Mycobacterium smegmatis* under conditions of nonreplication. *J. Bacteriol.* **192,** 3043–3054
42. Sanders, A. N., Wright, L. F., and Pavelka, M. S. (2014) Genetic characterization of mycobacterial L,D-transpeptidases. *Microbiology* **160,** 1795–1806
43. Schillinger, C., Boisguerin, P., and Krause, G. (2009) Domain interaction footprint: a multi-classification approach to predict domain-peptide interactions. *Bioinformatics* **25,** 1632–1639
44. Depuydt, M., Leonard, S. E., Vertommen, D., Denoncin, K., Morsomme, P., Wahni, K., Messens, J., Carroll, K. S., and Collet, J. (2009) A periplasmic reducing system protects single cysteine residues from oxidation. *Science* **326,** 1109–1111
45. Flores, A. R., Parsons, L. M., and Pavelka, M. S. (2005) Genetic analysis of the β-lactamases of *Mycobacterium tuberculosis* and *Mycobacterium smegmatis* and susceptibility to β-lactam antibiotics. *Microbiology* **151,** 521–532
46. Hugonnet, J. E., and Blanchard, J. S. (2007) Irreversible inhibition of the *Mycobacterium tuberculosis* β-lactamase by clavulanate. *Biochemistry* **46,** 11998–12004
47. Hugonnet, J. E., Tremblay, L. W., Boshoff, H. I., Barry, C. E., 3rd, and Blanchard, J. S. (2009) Meropenem-clavulanate is effective against extensively drug-resistant *Mycobacterium tuberculosis*. *Science* **323,** 1215–1218
48. Gouet, P., Courcelle, E., Stuart, D. I., and Métoz, F. (1999) ESPript: analysis of multiple sequence alignments in PostScript. *Bioinformatics* **15,** 305–308